Constraining long-term model predictions for woody growth using tropical tree rings

Global Change Biology

Xu, Xiangtao; van der Sleen, Peter; Groenendijk, Peter; Vlam, Mart; Medvigy, David et al

https://doi.org/10.1111/gcb.17075

Global Change Biology **WILEY**

Constraining long-term model predictions for woody growth using tropical tree rings

Xiangtao Xu[1] | Peter van der Sleen[2] | Peter Groenendijk[3] | Mart Vlam[2] | David Medvigy[4] | Paul Moorcroft[5] | Daniel Petticord[1] | Yixin Ma[1] | Pieter A. Zuidema[2]

[1]Department of Ecology and Evolutionary Biology, Cornell University, Ithaca, New York, USA

[2]Forest Ecology & Forest Management Group, Wageningen University, Wageningen, The Netherlands

[3]Department of Plant Biology, Institute of Biology, University of Campinas, UNICAMP, Campinas, SP, Brazil

[4]Department of Biological Sciences, University of Notre Dame, Notre Dame, Indiana, USA

[5]Department of Organismic and Evolutionary Biology, Harvard University, Cambridge, Massachusetts, USA

Correspondence
Xiangtao Xu, Department of Ecology and Evolutionary Biology, Cornell University, Ithaca, NY 14850, USA.
Email: xx286@cornell.edu

Abstract

The strength and persistence of the tropical carbon sink hinges on the long-term responses of woody growth to climatic variations and increasing CO_2. However, the sensitivity of tropical woody growth to these environmental changes is poorly understood, leading to large uncertainties in growth predictions. Here, we used tree ring records from a Southeast Asian tropical forest to constrain ED2.2-hydro, a terrestrial biosphere model with explicit vegetation demography. Specifically, we assessed individual-level woody growth responses to historical climate variability and increases in atmospheric CO_2 (C_a). When forced with historical C_a, ED2.2-hydro reproduced the magnitude of increases in intercellular CO_2 concentration (a major determinant of photosynthesis) estimated from tree ring carbon isotope records. In contrast, simulated growth trends were considerably larger than those obtained from tree rings, suggesting that woody biomass production efficiency (WBPE = woody biomass production:gross primary productivity) was overestimated by the model. The estimated WBPE decline under increasing C_a based on model-data discrepancy was comparable to or stronger than (depending on tree species and size) the observed WBPE changes from a multi-year mature-forest CO_2 fertilization experiment. In addition, we found that ED2.2-hydro generally overestimated climatic sensitivity of woody growth, especially for late-successional plant functional types. The model-data discrepancy in growth sensitivity to climate was likely caused by underestimating WBPE in hot and dry years due to commonly used model assumptions on carbon use efficiency and allocation. To our knowledge, this is the first study to constrain model predictions of individual tree-level growth sensitivity to C_a and climate against tropical tree-ring data. Our results suggest that improving model processes related to WBPE is crucial to obtain better predictions of tropical forest responses to droughts and increasing C_a. More accurate parameterization of WBPE will likely reduce the stimulation of woody growth by C_a rise predicted by biosphere models.

KEYWORDS
biomass production efficiency, tree ring, tropical forests, vegetation demography model, woody growth

---

1 | INTRODUCTION

Tropical forests are responsible for over half of global forest carbon sink (Pan et al., 2011). This large tropical carbon sink is predominantly due to carbon fixation and woody biomass production of tropical trees. One key determinant of the long-term integrity of this tropical forest carbon sink is the responses of tropical tree growth to the changing environment, such as increasing atmospheric CO_2 concentration (C_a), gradual climate change, and increasing climatic variability (Hubau et al., 2020; McDowell et al., 2020; Pugh et al., 2019). However, it remains challenging to quantify and disentangle the sensitivity of tree growth to climatic and C_a changes (Anderson-Teixeira et al., 2022; Bauman et al., 2022; Peltier & Ogle, 2020). The limited knowledge on environmental sensitivity of tree growth contributes importantly to the divergence of long-term tropical carbon dynamics simulated by terrestrial biosphere models (TBMs) (Bonan & Doney, 2018; Huntingford et al., 2013; Sitch et al., 2008).

A challenge to constrain simulations of tropical tree growth and its environmental sensitivity is the scarcity of tree growth data under a wide range of abiotic and biotic conditions, including climatic variability, long-term C_a increase, and tree size. Tree ring data can assist in filling the data gap by providing long-term, interannual records of tree growth (Anderson-Teixeira et al., 2022; Brienen et al., 2016; Zuidema et al., 2018). In addition, stable isotope signals in tree rings can further provide information on canopy photosynthesis and stomatal conductance as well as rooting depth (McCarroll & Loader, 2004), helping to interpret tree growth patterns. The increasing availability of tropical tree-ring data (Zuidema et al., 2022) provides opportunities for benchmarking tropical forest dynamics and environmental sensitivity of tropical tree growth in TBM simulations. While tree-ring data have been used to benchmark and calibrate TBMs (Anderegg et al., 2015; Jeong et al., 2021; Klesse et al., 2018; Rammig et al., 2015), these studies mostly aggregated data across trees and/or years to obtain stand-level or long-term average values of tree growth that can be matched with simulated values at the level of plant functional types (PFTs) produced by TBMs and dynamic global vegetation models (DGVMs). However, so far only few studies (Barichivich et al., 2021; Eckes-Shephard et al., 2021) have combined tree-ring data and output of TBMs with dynamic vegetation demography (Fisher et al., 2018; Friend et al., 1997; Medvigy et al., 2009).

Model biases in environmental sensitivity of tree growth can arise from either photosynthesis or woody biomass production efficiency (WBPE), which includes the efficiency of converting gross primary productivity (GPP) to net primary productivity (NPP) and the allocation of NPP to woody growth. Tree growth rates in mainstream TBMs are generally determined by carbon availability from photosynthesis (Fatichi et al., 2019), using biomass production efficiency derived from biome-specific parameter tuning (Collalti et al., 2020). The WBPE values applied in models are commonly insensitive to environmental factors (Fisher & Koven, 2020; Hickler et al., 2015; Xu & Trugman, 2021), leading to strong photosynthetic control of the interannual variability and long-term trends in tree growth. However, while tree growth requires photosynthetic carbon gain, it is not always limited by carbon

(Palacio et al., 2014; Sala et al., 2012). The decoupling of growth and photosynthesis is well manifested in vegetation responses to elevated CO_2: there is mounting evidence for increased GPP under higher C_a from leaf level to ecosystem and landscape level, but woody growth shows more complex responses (Cernusak et al., 2013; Norby & Zak, 2011; Walker et al., 2021). For example, a recent free-air CO_2 enrichment (FACE) experiment in a mature *Eucalyptus* forest in Australia found no apparent stem growth responses despite significant increases in GPP (Jiang et al., 2020). Similarly, sensitivity of stem growth to temperature and moisture variations was also reported to differ from that of GPP (Cabon et al., 2022; Doughty et al., 2015; Zweifel et al., 2021). These empirical results suggest that a constant WBPE as currently implemented in most models is likely not realistic. Therefore, consideration of the environmental sensitivity of WBPE offers a critical, yet often overlooked, opportunity to constrain model predictions of woody growth.

In this study, we compare simulations from a recent version of Ecosystem Demography model 2.2 that includes plant hydraulics (ED2.2-hydro, Xu et al., 2016, 2021) against tree-ring width and isotope-derived intercellular CO_2 (C_i) data from a tropical seasonal forest at Huai Kha Khaeng, Thailand (Groenendijk et al., 2015; Van Der Sleen et al., 2015; Vlam et al., 2014). After evaluating model performance to realistically represent contemporary forest structure and seasonality, we: (i) generate virtual tree ring series from model simulations based on the size distribution of in situ sampled trees, (ii) analyze temporal trends observed and simulated C_i and tree-ring width, and (iii) calculate the sensitivity of standardized stem growth (β_{SG}) to historical C_a changes and climatic variability from both observed and simulated tree-ring data (Figure 1). We then quantify the discrepancies between simulated environmental sensitivities of growth ($\Delta \beta_{SG}$) against those estimated from tree-ring records, which reflect model biases in the environmental sensitivities of WBPE. In all analyses we considered two PFTs: an early-successional and a late-successional life history strategy.

We used the above observations and analyses to test the following hypotheses: (H1) Modeled responses of C_i to long-term C_a increase are in line with empirical results from stable isotope in tree rings (Van Der Sleen et al., 2015); (H2) Modeled responses of stem growth to long-term C_a increase are higher than observations from tree ring width data (Groenendijk et al., 2015; Van Der Sleen et al., 2015) because WBPE in ED2.2-hydro does not decline under elevated C_a; (H3) Modeled responses of stem growth to interannual hydroclimatic variability are different from tree-ring observations because of unrealistic climatic sensitivity of WBPE in the model.

2 | MATERIALS AND METHODS

2.1 | Tree ring data and standardization

Tree ring data used in this study were collected in Huai Kha Khaeng (HKK) Wildlife Sanctuary in Thailand (15.60°N, 99.20°E). Vegetation in HKK is characterized as a seasonal tropical forest
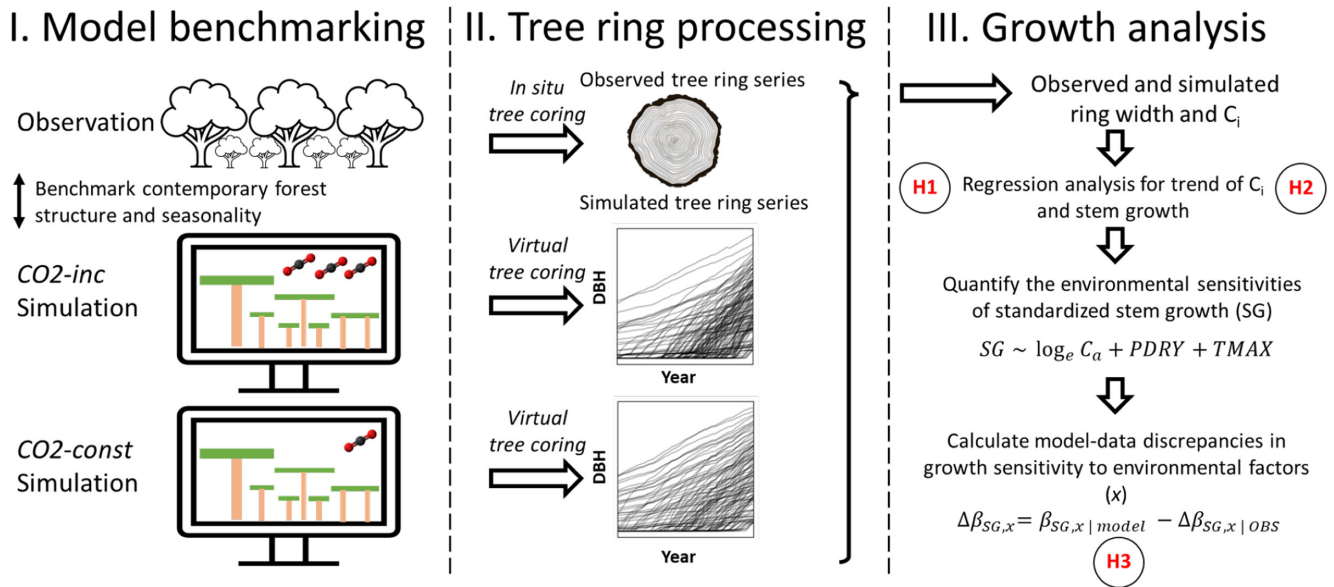
I. Model benchmarking | II. Tree ring processing | III. Growth analysis

FIGURE 1 Summary of research goals, hypotheses, and approaches in this study. First, two sets of model simulations with different C_a configurations (*CO2-inc* and *CO2-const*) were benchmarked with contemporary forest structure and dynamics (Model benchmarking). Second, simulated tree rings were extracted from individual tree-level model outputs from ED2.2-hydro. The virtual tree coring process was constrained by the tree size distribution of in situ tree coring to reduce sampling bias. Third, temporal trends of tree-ring width and C_i estimates from both observed and simulated tree rings were calculated with the consideration of tree size effect to evaluate H1 and H2. To evaluate H3, tree-ring records were further used to quantify standardized stem growth (SG) sensitivity to C_a, average maximum temperature (TMAX), and dry season precipitation (PDRY) for both observations and simulations.

(Bunyavejchewin et al., 2009) with an annual mean precipitation of 1473 mm and a 4- to 6-month dry season from November to April. Many species display dry season deciduousness or semi-deciduousness at HKK (Williams et al., 2008). Five species, *Toona ciliata*, *Melia azedarach*, *Chukrasia tabularis*, *Afzelia xylocarpa*, and *Neolitsea obtusifolia* were selected based on appearance of annual rings and relatively high local abundance. Roughly 100 trees above 5 cm diameter at breast height (DBH) were randomly selected and cored per species using 5-mm-diameter increment borers (Suunto, Finland and Haglöf, Sweden) in three to four directions per tree. This ecological tree ring sampling strategy includes individuals across extant diameter classes and provides more complete information on tree growth history within the tree community than sampling trees for climate reconstruction (dendroclimatology). Tree ring widths were measured using either a measuring table or high-resolution scans with quality control by cross-dating. More details of tree ring measurements can be found in Vlam et al. (2014).

The width of a tree ring is determined by (1) age- or size-dependent growth response that reflects tree ontogenetic changes and general microenvironmental change during plant life history and (2) growth responses to interannual and long-term environmental changes. Detecting long-term growth responses to CO_2 and climate requires removing the age- or size-dependent growth trend. This can be done not only by detrending individual tree-ring series (e.g., using flexible splines), but also by removing general growth-size relationships based on all tree-ring measurements together. The latter approach is preferred when analyzing growth trends over time

(Peters et al., 2015) and was implemented here. Specifically, we used regional curve standardization, a reliable technique to detect growth trends (Groenendijk et al., 2015; Peters et al., 2015). For each species, we therefore fitted a generalized Michaelis–Menten function (Equation 1) to all historical basal area increment (BAI), calculated from individual tree ring record, and DBH:

$$BAI = BAI_{max} \frac{DBH^a}{b + DBH^a}, \tag{1}$$

where three parameters, BAI_{max}, a, and b, determine the maximum value and curvature of growth-size relationships. This equation is equivalent to the commonly used three parameter generalized logistic growth function to model growth-size relationship (Groenendijk et al., 2015). We also compared this approach to generalized additive model (GAM) fits which did not assume a monotonic increasing relationship. The two approaches produced consistent growth-size relationships (Figure S1); however, GAM-derived growth curves were more variable for large DBH values due to data sparsity. Therefore, we used Equation (1) to standardize growth throughout our study. The standardized stem growth of individual i in year y ($SG_{i,y}$) was then calculated from observed BAI ($BAI_{obs,i,y}$) and estimated BAI based on the general growth-size relationship (Equation 1) for the functional group of the individual tree ($BAI_{est,i,y}$):

$$SG_{i,y} = \log_e BAI_{obs,i,y} - \log_e BAI_{est,i,y}. \tag{2}$$

SG is positive when stem growth is higher than expected based on the general ontogenetic growth pattern and is negative when stem growth is lower than expected. By removing the ontogenetic effects, SG from

Parameters	PFT-ES	PFT-LS
Species	*Toona ciliate*	*Chukrasia tabularis*
	Melia azedarach	*Afzelia xylocarpa*
		Neolitsea obtusifolia
Wood density (g cm^{-3})	0.5	0.75
Leaf turnover rate (year^{-1})	1.5	0.5
Specific leaf area (m^2 kgC^{-1})	25.8	16.1
$V_{c,max}$ (µmol m^{-2} s^{-1}, 15°C)[a]	27.9	22.0
R_{dark} (µmol m^{-2} s^{-1}, 15°C)	0.40	0.32
Leaf turgor loss point (MPa)	−1.56	−2.18
Xylem conductivity (kgH$_2$O m^{-2} s^{-1})	0.035	0.016
Xylem P50 (MPa)	−2.16	−3.25
b1Ht (dimensionless)[b]	1.59	1.57
b2Ht (dimensionless)[b]	0.46	0.44

TABLE 1 Key functional trait parameterization for the early-successional plant functional type (PFT-ES) and late-successional plant functional type (PFT-LS) in ED2.2-hydro for Huai Kha Khaeng.

[a]J_{max}:$V_{c,max}$ ratio is 1.797 at 15°C.

[b]Height = exp(b1Ht + b2Ht × log$_e$(DBH)).

different individual trees can be combined to evaluate temporal trends and environmental sensitivity in growth.

Carbon isotope ratios (δ^{13}C) were measured for wood sample from selected trees in each species at 8 cm and 27 cm DBH. The growth ring in which the tree reached 8 or 27 cm DBH was taken as midpoint, and the two growth rings before and after this midpoint were also sampled, resulting in a 5-year block wood sample. Cellulose was extracted for the wood samples and fed into an element analyzer coupled to a mass spectrometer (Sercon Hydra 20-20) at the Leicester Environmental Stable Isotope Laboratory, University of Leicester, UK. Estimates of intercellular CO_2 (C_i in ppm) were calculated from δ^{13}C (Van Der Sleen et al., 2015).

2.2 | Model description and simulation configuration

Ecosystem Demography v2.2 (ED2.2) is a TBM that tracks vegetation demographic dynamics and fine-scale carbon, water, and energy balances within ecosystems (Longo et al., 2019; Medvigy et al., 2009). In ED2.2, plant individuals with the same PFT, similar size, and disturbance history are grouped into cohorts. Vital demographic processes such as growth, mortality, and recruitment are simulated at cohort level at monthly time-step, based on the coupled carbon–water–energy dynamics simulated at sub-hourly time-step. To simulate the seasonal forest at HKK, we used ED2.2-hydro, a version of the model that has cohort-level plant hydraulics, which can better capture the diversity in seasonally dry tropical forest (Smith-Martin et al., 2020; Xu et al., 2016) and has been parameterized and benchmarked across a tropical moisture gradient (Xu et al., 2021). The stomatal model in ED2.2-hydro was based on the optimality theory (Katul et al., 2010) and included adaptations of marginal water-use efficiency under changes in water potential and CO_2 (Manzoni et al., 2013). ED2.2-hydro also implemented a light-driven

plasticity of key leaf functional traits, which is critical to simulating realistic forest size structure (Xu et al., 2021).

The carbon allocation to aboveground woody growth in ED2.2-hydro is determined by a series of processes, including leaf and fine root turnover, tissue maintenance respiration, reproductive investment, growth respiration, and aboveground-to-belowground partitioning. None of the model parameters controlling these processes (e.g., leaf turnover rate, reproductive allocation, etc.) are sensitive to C_a. In fact, most parameters are constant except that maintenance respiration parameters are dependent on temperature. Nutrient limitation influences carbon allocation and regulates tropical forest growth (Cunha et al., 2022; Fleischer et al., 2019; Waring et al., 2019; Wright, 2019). ED2.2 can estimate nutrient limitation on tree growth (Levy-Varon et al., 2019; Medvigy et al., 2019; Moorcroft et al., 2001); however, we did not enable nutrient limitation in this study because nutrient-related parameters and local biogeochemistry information were largely unknown. Cohort-level tree mortality is modeled as a function of growth and PFT (Camac et al., 2018).

We defined two PFTs along a general resource-use strategy axis to represent the diversity at the HKK site (Table 1). The early-successional PFT (PFT-ES) was characterized by acquisitive functional traits such as lower wood density, higher leaf turnover rate, higher photosynthetic capacity and dark respiration, higher hydraulic efficiency, and lower hydraulic safety compared with the more conservative late-successional PFT (PFT-LS). Wood density values were based on reported range of species at HKK (Nock et al., 2009) and was used to assign PFT to the five study species while another key trait in ED2.2-hydro, leaf turnover rate, was parameterized using default values in ED2.2-hydro that is representative of the range of leaf longevity in the tropics. Other ecophysiological parameters such as parameters for the Farquhar photosynthesis module were derived from wood density and leaf longevity based on previous trait meta-analysis (Longo et al., 2020; Xu et al., 2016). Height measurements

of all sampled trees were obtained using a digital hypsometer (Nikon Forestry 550) and were used to construct height allometry relationships (Table 1).

We conducted "near-bare-ground" simulations, that is, model initialization with a few small seedlings, since forest stand structure in pre-industrial era at HKK was unknown. The simulation started in the year 1600 with 0.5 m tall seedlings at a stem density of 0.1 individuals per meter squared for both PFTs. We ran the simulation to 2010, the year of in situ tree ring sampling, forced by monthly historical atmospheric CO_2 concentrations compiled by the Institute for Atmospheric and Climate Science at Eidgenössische Technische Hochschule in Zürich, Switzerland. In the simulation, we cycled climate data from the Princeton Global Meteorological Forcing (PGMF) 0.25° 3-hourly reanalysis dataset (Sheffield et al., 2006) that spans 1901 to 2012. The raw PGMF data were corrected using long-term in situ observations from the nearby Nakhon Sawan weather station. For each month, an additive correction factor was applied to temperature and relative humidity to ensure that the corrected reanalysis data had the same monthly seasonality as the station data. Similarly, a multiplicative correction factor was applied to precipitation to reduce biases in precipitation. Vapor pressure deficit was then calculated from the corrected temperature and relative humidity. The first 250 years (before 1850) was discarded as model spin-up. We also conducted another "near-bare-ground" simulation with the same configuration except that C_a was fixed at 285 ppm after 1850. This simulation was labeled as "*CO2-const*" while the previous simulation was labeled as "*CO2-inc*" (Figure 1). The difference between the two simulations reflected the net effect of historical Ca increase on tree growth in our model. Historical disturbance events such as storm and fire can also shape the sampling distribution and growth patterns in tree rings (Baker et al., 2005; Vlam et al., 2017) and model simulations. However, the exact timing and magnitude of those disturbances were unknown and thus could not be included in model simulations and we used a constant disturbance rate of 0.5% per year for both simulations based on the rainfall regime at HKK.

2.3 | Evaluation of simulated contemporary forest structure and seasonality

Simulated forest structure was benchmarked against forest census data at the 50 ha HKK plot (Bunyavejchewin et al., 2009). Average basal area and stem density of different DBH size classes from simulations in 1990 and 1991 were calculated and compared with field surveys conducted at the same time. We also compared simulated aboveground biomass with reported values for the site (Chave et al., 2008; Zuleta et al., 2023), which however showed large variation across studies due to uncertainty in allometry.

Given the strong seasonality of rainfall of the site, we further examined simulated GPP seasonality to benchmark model performance of seasonal water stress. This benchmarking can also shed lights upon the model's performance on GPP responses to interannual variability. Since no local carbon flux data were available, we compared average GPP seasonality with the flux tower data from a mixed deciduous forest at Mae Klong (14°34′34.2″ N, 98°50′37.2″ E), which is about 160 km to the south of HKK. Mae Klong has an annual rainfall of 1650, which is ~200 mm higher than HKK, and a strong rainfall seasonality similar to HKK (Huete et al., 2008). The flux tower sits on a mixed deciduous forest despite the forest is younger at Mae Klong. We extracted monthly GPP averaged over 2001–2004 from Huete et al. (2008) and compared the seasonality with simulated monthly GPP over the same period.

It should be noted that model parameters were not tuned or calibrated by either the observed forest structure or flux tower GPP. The evaluation aims to demonstrate our model configuration can generate reasonable forest structure and seasonality.

2.4 | Extracting tree rings from simulations

Although in situ tree ring data at HKK covered growth history of a wide range of tree sizes (5–150 cm), the size distribution of the sampled trees was different from that of the whole forest. Simply comparing the full growth history of all individuals from simulations with observations would suffer from biases due to the different size distribution (Jeong et al., 2021). To make a fair comparison, we selected simulated tree cohorts present at the end of 2010 using a stratified sampling strategy to generate a similar tree size distribution as in situ tree ring collection for each PFT (Figure S2). The in situ tree ring data contained 151 trees for PFT-ES and 307 trees for PFT-LS. Based on the observed DBH distribution, 47 cohorts were selected for PFT-ES and 86 cohorts were selected for PFT-LS from the output of *CO2-inc* simulation while the cohort sample size was 44 for PFT-ES and 65 for PFT-LS from the output of *CO2-const* simulation. Kolmogorov–Smirnov tests implied that the size distribution of simulated cohorts is not different for the size distribution of in situ data for either PFT-ES or PFT-LS.

To back-trace individual cohort growth history from standard model output, we generated and tracked a unique label for each new cohort in the model. In a model simulation, two cohorts can be fused if they are very similar in size and microenvironment for the sake of computational efficiency. Also, a single cohort splits into two once its leaf area index exceeds a certain threshold. The cohort splitting helps to avoid biases due to the model assumption that leaves within a cohort receive the same amount of light. During cohort fusion, the growth history of the smaller cohort (often less abundant) is discarded. During cohort splitting, each new cohort is assigned a new label that is linked to the original label. In this way, we could extract a unique full growth record for each extant cohort at any point of a simulation that is most consistent with the observed tree-ring sampling.

For each simulated tree ring, we also calculated the average sub-hourly C_i weighted by GPP within each growing season. We then extracted the average C_i for the 5–10 cm and 25–30 cm rings, which are directly comparable to the observed 8 and 27 cm C_i values described in Section 2.1.

2.5 | Temporal trends of C_i and stem growth

We compared the temporal trends of C_i and growth for each PFT from both observed and simulated tree-ring records using ordinary least squares (OLS) regression to evaluate hypothesis H1 and H2. We removed size effect when calculating trends since size effect arising from various ontogenetic and microenvironmental sources can bias temporal signals (van der Sleen et al., 2017). In the regression analysis for C_i, we modeled size as a categorical variable which influences the mean of C_i but has no interactive effect with time, since there were only two size categories for C_i data.

We estimated the nonlinear size dependence of tree growth by fitting the generalized Michaelis–Menten function (as described in Equation 1) to the observed and simulated growth records, respectively. We then calculated the temporal trends of SG, which resulted from growth deviations from the average growth-size relationships (as described in Equation 2). We also conducted the same trend analysis using GAM to standardize stem growth to examine whether the trend analysis was influenced by the choice of growth standardization. We further conducted a size class-specific trend analysis, following Groenendijk et al. (2015), to investigate whether long-term growth trends depended on tree size. We used a 20 cm window to ensure enough sampling for each size class from 10 to 110 cm DBH. We assessed the likelihood of "juvenile selection bias", which could lead to artificial negative growth trend, using a 90%-quantile regression.

2.6 | Analysis of growth sensitivity to C_a and climate

We estimated the sensitivity of SG to C_a and key climatic factors, using the following equation:

$$SG = \beta_{SG,C_a} \log_e C_a + \beta_{SG,PDRY} PDRY + \beta_{SG,TMAX} TMAX + constant,$$

(3)

where C_a indicates annual mean atmospheric concentration, *PDRY* indicates dry season total rainfall of the current year, and *TMAX* indicates annual mean maximum daily temperature. The two climatic variables were selected based on Vlam et al. (2014), which suggested dry season precipitation and maximum temperature were more correlated with growth at HKK. Here, dry season was defined as previous year November to current year April. C_a was log-transformed following Walker et al. (2021) and SG was also log-transformed growth (as indicated in equation 2). For the *CO2-const* simulation, we still used realistic historical atmospheric CO_2 concentration as C_a, expecting the regression coefficient would be nonsignificant. Although ontogenetic effect was removed when calculating SG, we applied the regression for large (DBH ≥ 60 cm) and relatively small (DBH < 60 cm) trees because SG sensitivity to environment can depend on size classes which have different microenvironment. The DBH threshold was chosen because growth trends were more

consistent after 60 cm in observations during our size class analysis. The regression coefficients and confidence interval for C_a, *PDRY* and *TMAX* (β_{SG,C_a}, $\beta_{SG,PDRY}$, and $\beta_{SG,TMAX}$) were extracted and compared between observation and simulations across PFT and size groups to evaluate hypotheses H2 and H3. We did not conduct the sensitivity analysis for C_i because observed C_i data was 5-year average, and the temporal resolution was too coarse to robustly investigate responses to interannual variability in climate.

We further calculated the model-data discrepancy in stem growth sensitivity as the difference between β_{SG} derived from simulated tree rings and the corresponding sensitivity derived from in situ tree rings:

$$\Delta\beta_{SG,C_a} = (\beta_{SG,C_a,CO2-inc} - \beta_{SG,C_a,CO2-const}) - \beta_{SG,C_a,OBS}, \quad (4.1)$$

$$\Delta\beta_{SG,PDRY} = \beta_{SG,PDRY,CO2-inc} - \beta_{SG,PDRY,OBS}, \quad (4.2)$$

$$\Delta\beta_{SG,TMAX} = \beta_{SG,TMAX,CO2-inc} - \beta_{SG,TMAX,OBS}. \quad (4.3)$$

Positive or negative $\Delta\beta_{SG}$ values imply model predicted higher or lower stem growth sensitivity compared with tree rings, respectively. When calculating $\Delta\beta_{SG,C_a}$ (Equation 4.1), we subtracted β_{SG,C_a} from the *CO2-inc* simulation by β_{SG,C_a} of the *CO2-const* simulation because any apparent C_a sensitivity from the *CO2-const* simulation must come from the collinearity between historical C_a trend and transient decadal dynamics in model simulations (e.g., forest recovering from earlier disturbances). The transient dynamics was less of a concern for PDRY and TMAX since they had very weak temporal trend compared with interannual variability. Therefore, the correction was not necessary. We estimated the uncertainty of all $\Delta\beta_{SG}$ values by bootstrapping the distribution of β_{SG} values derived from OLS regressions. Calculation of growth sensitivities was conducted for all combinations of two size categories (<60 cm, ≥60 cm) and two PFTs.

The rate of stem growth is the product of GPP and WBPE. Therefore, $\Delta\beta_{SG}$ can arise from discrepancies in either GPP or WBPE sensitivities. In this study, we focused on WBPE sensitivities and compared $\Delta\beta_{SG,C_a}$ in our study with reported WBPE responses to elevated CO_2 at the EucFACE experiment in Australia (extended fig. 7 from Jiang et al., 2020). In particular, we calculated the $\Delta\beta_{SG,C_a}$ value if the observed WBPE response from the FACE experiment would have been included in our model. No field-based estimates of WBPE sensitivity to interannual variation in temperature and precipitation were available for tropical forests and therefore a quantitative evaluation of $\Delta\beta_{SG,PDRY}$ and $\Delta\beta_{SG,TMAX}$ was not possible. We assumed model biases in GPP sensitivities were generally negligible because TBMs based on similar photosynthesis modules largely captured observed GPP responses to C_a and climatic variability (Piao et al., 2020; Walker et al., 2021). The assumption was indirectly evaluated by comparing the long-term C_i trend between model and simulation (for C_a sensitivity) as well as GPP seasonality between model and the Mae Klong flux tower (for water sensitivity).

In analyses of trends and sensitivity, we only used observations and simulations after 1950 when the climate records are more available and trustworthy. All statistical analysis was conducted with the

statsmodels 0.13.2 package (Seabold & Perktold, 2010) in Python 3.10.

3 | RESULTS

3.1 | Benchmarking simulated contemporary forest structure and seasonality

The field census at HKK 50 ha plot in the early 1990s (Bunyavejchewin et al., 2009) reported a mean (±SD) basal area of $28.64 \pm 5.7\,m^2\,ha^{-1}$ for trees >10 cm DBH, $20.33 \pm 5.43\,m^2\,ha^{-1}$ for ≥30 cm trees, and $5.57 \pm 4.46\,m^2\,ha^{-1}$ for ≥100 cm trees. Both the *CO2-inc* and *CO2-const* simulations generated basal area values within the reported range; however, the *CO2-inc* simulation had higher basal area values closer to field observations, especially for ≥100 cm trees ($5.95\,m^2\,ha^{-1}$, Figure 2a). Stem densities in the 10–30, 30–100, and >100 cm size classes were 438, 83, and 5.6 individuals per hectare in the field data. The corresponding stem densities in the *CO2-inc* simulation were 277.4, 87.4, and 6.7 individuals per hectare respectively indicating underestimation of the density of small trees (10–30 cm). The *CO2-const* simulation had stem densities of 262.0, 84.4, and 3.4 individuals per hectare respectively in the three size classes indicating underestimation of the density of both small (10–30 cm) and large (≥100 cm) trees (Figure 2b). The predicted aboveground biomass was $344\,Mg\,ha^{-1}$ in the *CO2-inc* simulation, which was higher than the value of $264\,Mg\,ha^{-1}$ in the *CO2-const* simulation as expected. Previous studies (Chave et al., 2008; Zuleta et al., 2023) reported values ranging from 200 to $300\,Mg\,ha^{-1}$ with large uncertainties depending on height and biomass allometry used given that no local biomass allometry was available. In particular, the lower end estimate was based on allometry fitted with three dry forest stands with a maximum DBH of 63.4 cm (Chave et al., 2005), which does not represent the HKK site well.

ED2.2-hydro predicted a strong seasonality in GPP (Figure 2c) due to stomatal and phenological responses to rainfall seasonality. GPP from the *CO2-inc* simulation peaked in the early wet season (June–July, $\sim11\,gC\,m^{-2}\,day^{-1}$) and was lowest in late dry season (March–April). The *CO2-const* simulation showed very similar seasonality with consistently lower GPP values. Flux tower data at Mae Klong exhibits weaker GPP seasonality with a similar timing of high and low values because the forest contains a larger fraction of evergreen species than the main study forest, which is almost fully deciduous. Mean annual GPP of the Mae Klong data was $7.53\,gC\,m^{-2}\,day^{-1}$ while the *CO2-inc* simulation predicted a value of $7.01\,gC\,m^{-2}\,day^{-1}$ and the *CO2-const* simulation predicted $5.65\,gC\,m^{-2}\,day^{-1}$, consistent with its underestimation of basal area and stem density (Figure 2a,b).

3.2 | Temporal trends of C_i and growth

The isotope-derived C_i data from observed tree rings increased from 1950 to 2010 at a rate of 80–95 ppm per 100 years for both PFTs (Figure 3). C_i trend of the *CO2-inc* simulation was slightly lower than the observed trend, which nevertheless fell inside the confidence interval of the observed C_i trend. In contrast, the C_i trend of the *CO2-const* simulation, in which atmospheric CO_2 concentration was held constant at 285 ppm, was not significantly different from zero for PFT-ES and slightly negative for PFT-LS. Canopy stomatal conductance also declined in *CO2-inc* simulation but remained relatively constant in the *CO2-const* simulation (Figure S3f). Overall, the comparison suggests that our model could capture long-term CO_2 effect on leaf-level gas exchanges.
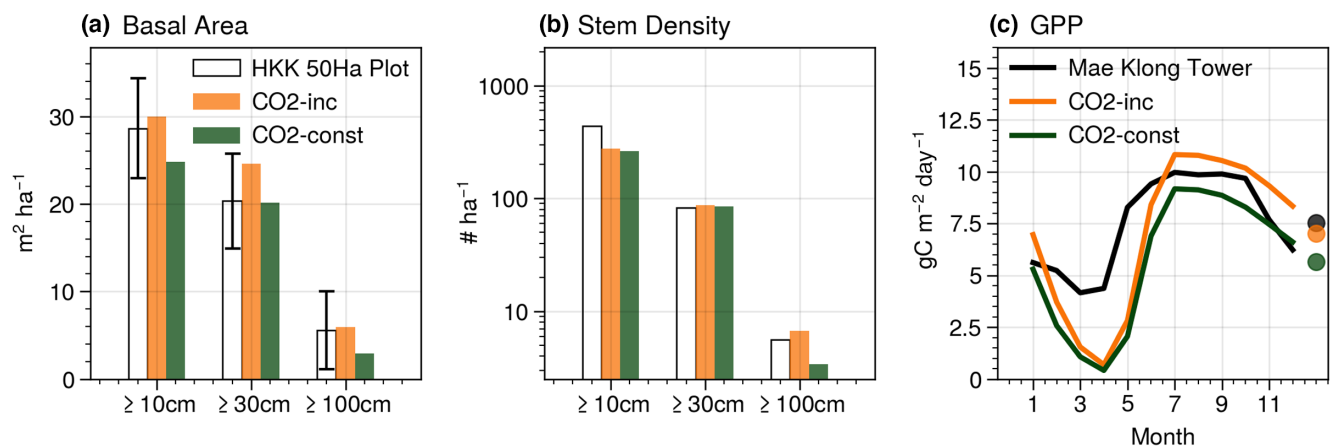

FIGURE 2 Comparison of contemporary ecosystem-level variables between simulations and various independent observations. (a, b) Stand basal area and stem density across tree size groups from ground census data at the Huai Kha Khaeng (HKK) 50 ha forest plot and ED2.2-hydro simulations (white bars) driven by different Ca scenarios (colored bars). Error bars reflect standard deviation of basal area across subplots within the HKK plot. (c) Average GPP seasonality from ED2.2-hydro simulations and the Mae Klong flux tower site located in a mixed deciduous forest similar to HKK. Colored dots indicate the mean annual GPP from the three different data sources.
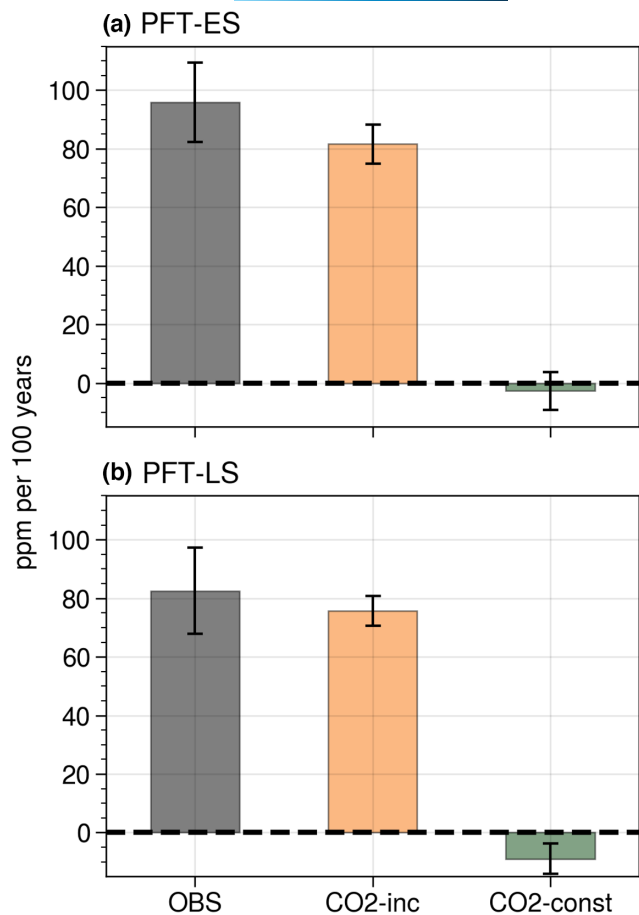
(a) PFT-ES

(b) PFT-LS

FIGURE 3 Temporal trends of C_i based on observed and simulated tree ring data from 1950 to 2010 for two plant functional types: early-successional (PFT-ES, a) and late-successional (PFT-LS, b). Tree size effect was removed when estimating the trend values.

Basal area increment from tree ring observations increased rapidly with tree DBH until about 40–50 cm for both PFT-ES and PFT-LS, beyond which average BAI started to level off (Figure 4a,b). The upper value of BAI was about 75 cm² year⁻¹ for the PFT-ES and about 55 cm² year⁻¹ for PFT-LS. BAI from the *CO2-inc* simulation closely matched the BAI–size relationship from tree rings, suggesting the model can capture the general growth-size relationship. The simulation underestimated growth of trees smaller than 50 cm for both PFTs and overestimated growth for trees bigger than 60 cm for PFT-ES. BAI from the *CO2-const* simulation was consistently lower than the observations by about 10%–30%. Both simulations predicted higher growth rates for the smallest trees (DBH < 15 cm) of PFT-LS.

Standardized stem growth of observed tree rings (Figure 4c,d) showed significant negative trends for both PFTs with a more negative trend for PFT-LS, which is consistent with previous analyses at the site (Groenendijk et al., 2015; Van Der Sleen et al., 2015). In contrast, simulated tree ring records showed significantly positive growth trends for PFT-ES in both *CO2-inc* and *CO2-const*. Using alternative stem growth standardization methods generated comparable growth trends (Figure S4). The positive growth trend from the *CO2-const* simulation was unexpected since no CO₂ increase

was included. The transient model behavior was likely caused by a drought period around 1980 in the meteorological forcing that led to decline in productivity and a subsequent recovery in model simulations (Figure S3). However, the positive growth trend in *CO2-inc* is larger than the trend in *CO2-const* (Figure 4c), implying an overall growth boosting effect of higher CO₂ in the model. For PFT-LS, the growth trend in *CO2-const* was not significantly different from zero as expected, implying a weaker response to the 1980 dry period due to its more conservative and resistant hydraulic traits compared with PFT-ES (Table 1). Interestingly, the growth trend of PFT-LS in *CO2-inc* was also nonsignificant, which was due to a strong size-dependent growth response to CO₂ (Figure 4e,f) as explained below.

The growth trends varied across size classes (Figure 4e,f). In observed tree rings, growth trends were negative for <60 cm trees and were nonsignificant (PFT-ES) or positive (PFT-LS) for ≥60 cm trees. Simulated tree rings also showed a positive size dependence of growth trends until 50–60 cm size classes although the growth trends values were generally higher than the corresponding observed values. It is also noteworthy that, for ≥60 cm of PFT-LS, the simulated growth trends became comparable with observed growth trends. Therefore, the difference in overall growth trends (Figure 4d) between observation and simulations was mainly caused by small trees. These size-specific trends did not change when an alternative growth standardization method was used (Figure S4). Furthermore, the growth trends from observed tree rings remained negative when we used the 90th quantile regression and the relative relationships between observed and simulated growth trends also remained the same (Figure S5). Therefore, the negative trend was unlikely to be caused by "juvenile selection bias" (cf. Groenendijk et al., 2015).

3.3 | Sensitivity of standardized stem growth to C_a and climate

The partial sensitivity of standardized stem growth to C_a (β_{SG,C_a}) showed consistent patterns with the growth trend analysis across PFT and size classes. For PFT-ES, β_{SG,C_a} derived from observed tree-ring data was negative for both <60 cm and ≥60 cm trees, respectively, while β_{SG,C_a} was positive for all size classes in both the *CO2-inc* simulation and *CO2-const* simulations (Figure 5a,b). As mentioned above, the positive β_{SG,C_a} in the *CO2-const* simulation in part reflected a transient temporal trend of PFT-ES. This also implies that β_{SG,C_a} of the *CO2-inc* simulation was likely overestimated and the difference between the *CO2-inc* and *CO2-const* values was a better estimate of β_{SG,C_a} for our model. In contrast, for PFT Late (Figure 5c,d), the *CO2-const* β_{SG,C_a} was not significantly different from zero as expected, while the in situ and *CO2-inc* β_{SG,C_a} was negative for <60 cm trees but positive for ≥60 cm trees.

The growth sensitivity to climate varied more between the two PFTs than across tree size classes. In situ tree-ring data showed significantly positive growth sensitivities to dry season rainfall ($\beta_{SG,PDRY}$) for both <60 cm and ≥60 cm size classes of PFT-ES

FIGURE 4 Size dependence and temporal trends in observed and simulated tree-ring growth records from 1950 to 2010 for the two plant functional types: early successional (PFT-ES) and late successional (PFT-LS). (a, b) Average basal area increment (BAI) changes with size, estimated from generalized Michaelis–Menten model fitting. (c, d) Temporal trends of standardized stem growth (SG). (e, f) Standardized stem growth (SG) trends for different tree size classes. For panels (c)–(f), the unit denotes the trend in standardized growth as defined in Equation (2). A value of 1 per 100 years indicates growth has increased by 2.72 times in a century or 1.64 times from 1950 to 2010. Similarly, a value of −1 per 100 years indicates growth in 2010 is 1.64 times less than growth in 1950.
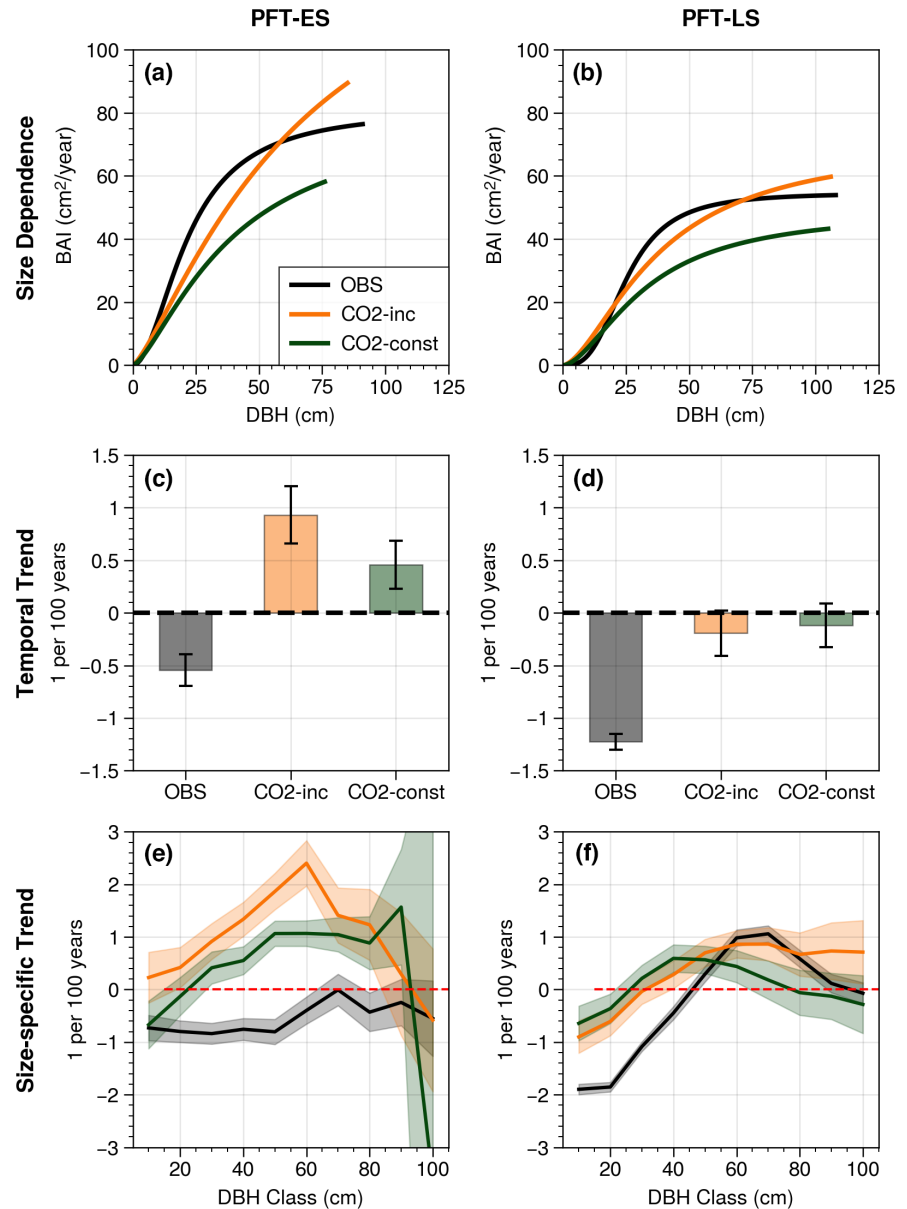
(Figure 5e,f). In contrast, the growth of PFT-LS trees was not sensitive to interannual variability in dry season rainfall (Figure 5g,h). Similarly, growth sensitivities to maximum temperature ($\beta_{SG,TMAX}$) were significantly negative for PFT-ES, but was nonsignificant for PFT-LS (Figure 5i–l). The *CO2-inc* simulation generated significantly positive $\beta_{SG,PDRY}$ and negative $\beta_{SG,TMAX}$ values for all PFT-size classes except for the $\beta_{SG,PDRY}$ of ≥60 cm PFT-ES trees, which was nonsignificant (Figure 5e–l). The magnitude of simulated growth climatic sensitivity generally agreed with the values derived from in situ tree-ring data for PFT-ES although there was overestimation for $\beta_{SG,TMAX}$. Meanwhile, the model greatly overestimated growth climatic sensitivity for PFT-LS. The *CO2-inc* and *CO2-const* simulations generated comparable $\beta_{SG,PDRY}$ and $\beta_{SG,TMAX}$ values suggesting higher C_a did not change growth responses to temperature and moisture in the model. Similar to our trend analysis results, the estimated environmental sensitivities of growth showed similar values and relationships across observations and

models, when alternative growth standardization method was used (Figure S6).

Based on Equation (4.1), we calculated the discrepancies in sensitivities between model and tree-ring data. We found that differences in growth sensitivity to C_a ($\Delta \beta_{SG,C_a}$) were positive for all PFT-size classes with more positive values for <60 cm trees (Figure 6a), implying higher sensitivities from our model than from tree-ring data. Yet, all $\Delta \beta_{SG,C_a}$ estimates had large uncertainties. In comparison, the EucFACE experiment reported ~21% reduction in WBPE under 38% C_a increase in a more open Australian mature *Eucalyptus* forest. This WBPE response is equivalent to a $\Delta \beta_{SG,C_a}$ of 0.81, a value close to the estimated $\Delta \beta_{SG,C_a}$ for big PFT-LS trees with comparable uncertainty (Figure 6a), suggesting that the lower observed WBPE under elevated CO_2 accounts for a large share of model biases in growth sensitivity for late-successional canopy trees.

In similar fashion, we also quantified the model biases in growth sensitivities to climate (Figure 6b,c). For both size classes of PFT-LS,
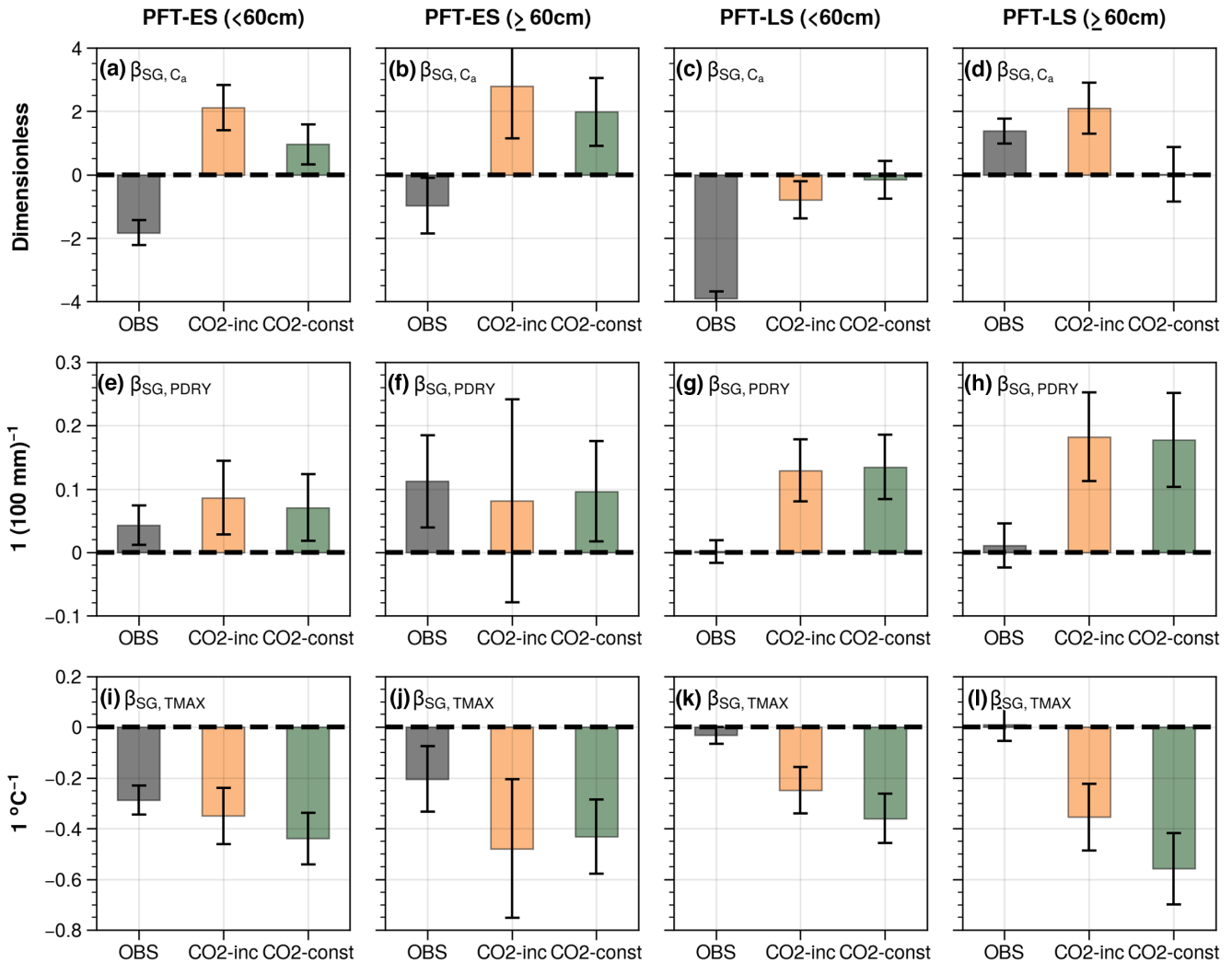
FIGURE 5 Partial sensitivities of standardized stem growth (SG) to (a–d) the logarithm of atmospheric CO_2 concentration (C_a), (e–h) dry season rainfall (PDRY), and (i–l) annual mean maximum daily temperature (TMAX). All sensitivities are shown for both observed and simulated tree-ring records. Each column of panels presents regression analyses using Equation (3) for a combination of plant functional type and size class (indicated in column label). The units indicate changes in standardized growth, defined in Equation (2), per unit change in C_a (log-transformed), PDRY, and TMAX. Error bars in each panel represent 95% confidence interval from OLS regression. To reasonably estimate growth sensitivity to C_a for the *CO2-const* simulation, we used historical atmospheric CO_2 concentration in the regression analysis although CO_2 was set as constant at 285 ppm (see Section 2.6 for details).

$\Delta\beta_{SG,PDRY}$ was significantly positive and $\Delta\beta_{SG,TMAX}$ was significantly negative. In contrast, for PFT-LS, $\Delta\beta_{SG,PDRY}$ was not significantly different from zero for PFT-ES. $\Delta\beta_{SG,TMAX}$ of ≥60 cm PFT-ES trees was comparable to the value of PFT-LS but had large uncertainty while $\Delta\beta_{SG,TMAX}$ for <60 cm PFT-ES trees was small and not significantly different from zero.

4 | DISCUSSION

4.1 | Reduced woody biomass production efficiency under long-term C_a increase

Previous benchmarking of TBMs' sensitivity to elevated C_a is mostly based on manipulative experiments that do not extend beyond the

decadal time scale (Fleischer & Terrer, 2022; Hickler et al., 2015). Our study provides novel model constraints based on tree-ring data that records multi-species growth responses to gradual C_a increases over 60 years. Trend analysis over simulated and observed tree ring data supported hypothesis H1 and H2 that ED2.2-hydro could capture C_i trend but not growth trends because a positive CO_2 effect on photosynthesis is included in its photosynthesis-stomata module, which improves growth under a source-driven growth scheme. Furthermore, we found that model overestimation of the stem growth trend at Huai Kha Khaeng can be largely explained by a high and invariant WBPE. These results lend further support to limited CO_2 fertilization effects on tropical vegetation biomass production (Fleischer et al., 2019; Fleischer & Terrer, 2022; Jiang et al., 2020; Terrer et al., 2019). In particular, the magnitude of WBPE decline for ≥60 cm late-successional trees (~50% of total biomass in simulation) is comparable to observed
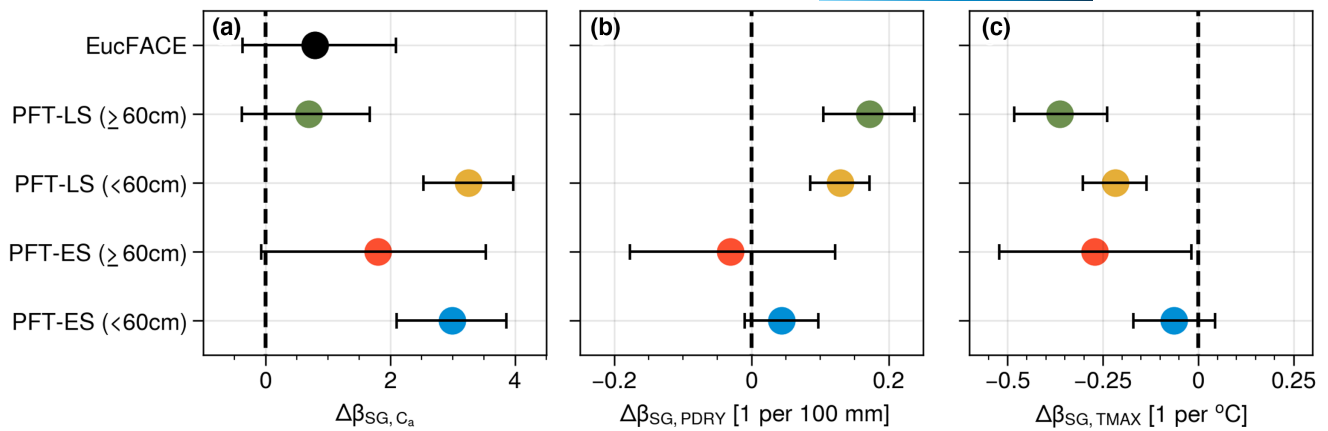
FIGURE 6 Differences in climatic and atmospheric sensitivities between model and tree-ring data. Differences are shown for stem growth (SG) sensitivity to (a) atmospheric CO_2 concentration (C_a), (b) dry season rainfall (PDRY), and (c) annual mean daily maximum temperature (TMAX). Error bars indicate 95th confidence interval calculated from bootstrapping. Positive values indicate that the modeled sensitivities are higher than those obtained from tree-ring data. In panel (a), woody biomass production efficiency (WBPE) responses to elevated CO_2 were obtained from the EucFACE experiment (see Section 2.6 for details).

WBPE decline at the EucFACE experiment (Jiang et al., 2020) while the estimated WBPE decline for early-successional trees and <60 cm trees was even stronger. This novel model constraint from tree ring data suggested absolute WBPE should have decreased from 0.2 to 0.15 (or ~25% relative decrease) under historical C_a increase in our study period (Figure 7a). A simple extrapolation of our results to the recently established AmazonFACE experiments, which plans to raise C_a from 410 to 600 ppm (Grossman, 2016), would predict a relative WBPE reduction of 25% (±30%) for ≥60 cm late-successional trees, 48% (±39%) for ≥60 cm early-successional trees, and close to 70% (±10%) for <60 cm trees of both PFTs. Our analysis could not distinguish the contribution of carbon use efficiency (CUE=NPP:GPP) and plant NPP allocation to WBPE reduction under higher CO_2. We suggest that increases in belowground carbon investment into fine roots (which typically have high rates of turnover), and priming (in order to alleviate nutrient limitation) likely dominate these responses, based on available knowledge from experiments, modeling, and meta-analysis (Collalti & Prentice, 2019; Fleischer et al., 2019; Jiang et al., 2020; Vicca et al., 2012).

Our attribution of model biases in growth sensitivity to CO_2 hinges on the assumption of relatively small biases in simulated GPP sensitivity to C_a. GPP can be approximated as multiplication of C_i and leaf carboxylation capacity (Vcmax). Although Vcmax was observed to decline under CO_2 enrichment experiment, the magnitude of decline was around 10% or smaller for tree species when CO_2 was elevated for 200 ppm or more (Ainsworth & Long, 2005). Particularly, recent experiments for tropical tree species (Fauset et al., 2019; Slot et al., 2021) reported insignificant to 10% decline in Vcmax for CO_2 increases that were considerably larger (400 ppm) than experienced by trees in our study (80 ppm). Therefore, the consistent C_i trends between observed and simulated tree rings (Figure 3) under a relatively constant Vcmax provides indirect support of the assumption that biases in simulated GPP sensitivity to C_a were small. Unfortunately, no direct measurements of whole-stand tropical forest GPP responses to CO_2 rise are available to verify this. The sensitivity of simulated GPP (normalized to per leaf area to remove the influence of transient dynamics in leaf area index) to logarithm C_a ($\beta_{GPP,aCO2}$) from our *CO2-inc* simulation was 0.60 ± 0.09 (equivalent to ~50% increase for a doubling of C_a) estimated with OLS regression. When accounting for Vcmax acclimation to higher CO_2, for example, 2% from 1950 to 2010, this would only slightly reduce our estimated $\beta_{GPP,aCO2}$ by 0.08. Our estimated $\beta_{GPP,aCO2}$ is very close to the mean value of a meta-analysis over field and greenhouse experiments (0.65 with a large standard deviation of 0.84, Walker et al., 2021) and a recent model-based estimate (47% based on a doubling C_a, Haverd et al., 2020), but it is higher than the sensitivity calculated from the recent EucFACE study ($\beta_{GPP,C_a}=0.34$). Overall, we argue that WBPE changes have a dominant effect on forest woody production responses to elevated CO_2. Further studies, such as the new AmazonFACE experiment, are necessary to disentangle and better quantify the effects of C_a rise on GPP and WBPE in tropical forests.

In our analysis, we also assumed the scaling between BAI and woody biomass production, which is sensitive to the relationship between DBH and height, did not change under increasing C_a. Ideally, repeated, paired measurements of DBH and height would be used to determine the sensitive of DBH-height allometry to C_a. Such measurements are not common and were unavailable at our study site. However, at one FACE experiment in a temperate forest, elevated C_a caused *Pinus taeda* trees to be taller for a given DBH (Kim et al., 2020). This is a possible alternative hypothesis for model overestimation in growth responses to C_a although further studies on the magnitude of tropical tree allometry responses to C_a changes are needed to evaluate the hypothesis. In addition, changes in allometry might be possible for smaller trees, which prioritize height growth due to increased shading (Holbrook & Putz, 1989) under higher C_a, resulting in a lack of stem growth increase despite higher biomass production. This light-driven allometry plasticity is not included in our model and might explain the larger model-data discrepancies in growth trend and C_a sensitivity for smaller size classes (10–60 cm, Figures 4e,f and 6a).
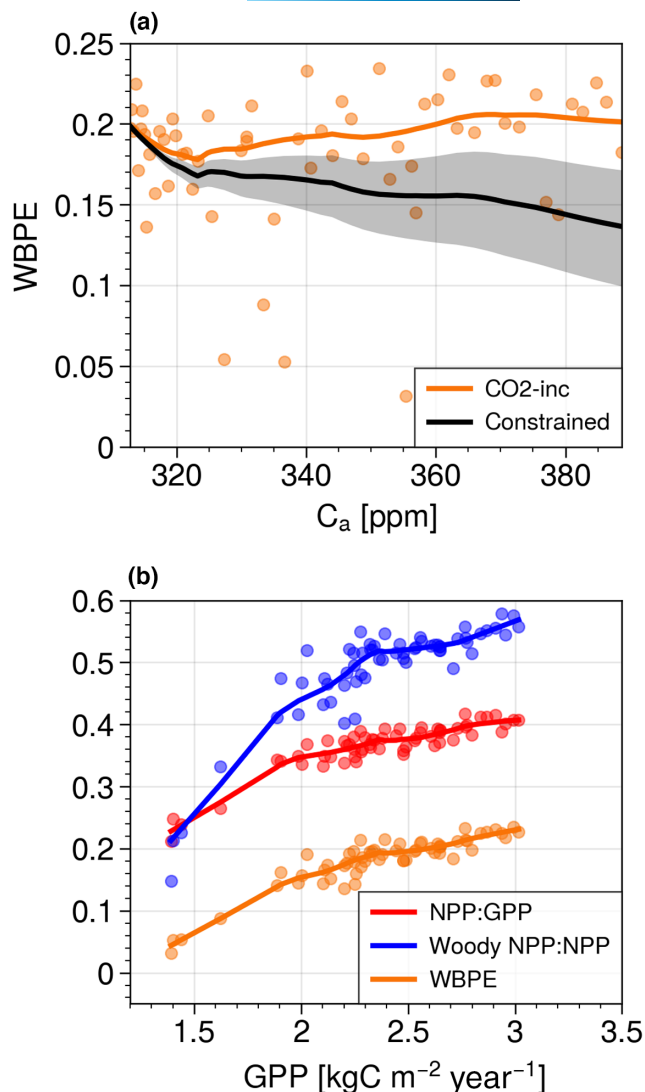
FIGURE 7 (a) Magnitude of estimated woody biomass production efficiency (WBPE) decline constrained by tree ring data. Orange dots represent annual WBPE as a function of atmospheric CO_2 concentration (C_a) predicted by the *CO2-inc* simulation. Solid orange line results from LOWESS (locally weighted scatterplot smoothing). Solid black line indicates estimated WBPE to match stem growth from simulation and tree ring observations (constrained). It is calculated using the orange line and a biomass-weighted average $\Delta\beta_{SG,C_a}$ as shown in Figure 6a. Grey shading indicates the range of estimated WBPE across plant functional type-size class as defined in Figure 6. (b) Decline of ecosystem-level carbon use efficiency (NPP:GPP, red), woody NPP allocation (woody NPP:NPP, blue) and WBPE (equal to the product of the previous two values, orange) with GPP in the *CO2-inc* simulation. Each dot represents relative change of CUE or woody NPP allocation compared with their respective maximum values against the GPP of the year. Solid lines are results from LOWESS smoothing to facilitate comparison.

4.2 | Increased woody biomass production efficiency in hot and dry years

ED2.2-hydro predicted significant positive growth sensitivity to dry season rainfall and negative growth sensitivity to maximum

temperature for the late-successional PFT, while tree-ring data showed no growth sensitivity to interannual variability in these climatic variables (Figure 5e–l). In contrast, for the early-successional PFT, simulated climatic sensitivity of growth was comparable to the observed values. Thus, we found support for our hypothesis H3 for the late-successional PFT only. Given that simulated growth is mostly driven by carbon availability, this comparison suggests source-driven growth scheme in our model might well capture growth sensitivity to hydroclimatic variations for early-successional species but would overpredict the sensitivity for late-successional species in this seasonally dry tropical forest. This finding seems to contrast recent results based on flux towers and tree ring data in temperate forests (Cabon et al., 2022), which showed that responses to climatic variation are weaker and delayed in woody growth compared to photosynthesis. Meanwhile, our results do not contradict field observations in tropical forests: sensitivity of tropical tree growth to moisture is reported to range from weak negative to strong positive (Zuidema et al., 2022) and species with higher wood density and hydraulic safety can maintain growth in dry years (Mendivelso et al., 2013; Xu et al., 2016).

The model-data discrepancy in growth sensitivity resulted in positive $\Delta\beta_{SG,PDRY}$ values and negative $\Delta\beta_{SG,TMAX}$ values (Figure 6a), which most likely arose because WBPE in our model was too low in hot and dry years. In our *CO2-inc* simulation, carbon use efficiency (NPP:GPP) declined from 0.4 to ~0.2 in hot and dry (low GPP) years (Figure 7b) because autotrophic respiration in the model does not decline much in drought unless significant canopy loss occurs. In addition, NPP allocation to woody growth in the model also declined from ~0.55 to 0.2–0.3 during drought because the model always prioritizes leaf and fine root growth and replacement over woody growth: ED2.2-hydro accumulates NPP into a nonstructural carbohydrate storage pool and only allows for woody allocation when the storage pool reaches a threshold. As a result, WBPE declined from over 0.2 to below 0.1. Although studies looking at longer-term forest responses to water stress reported that forest production efficiency decreased under multi-year throughfall exclusion experiment (Metcalfe et al., 2010) and is generally lower in hotter and drier regions (Collalti et al., 2020), WBPE was observed to have temporarily increased during droughts when woody production remained at the level of normal years despite a reduction in GPP in Amazonian forests (Doughty et al., 2015). This observed short-term increase in WBPE during drought years in the Amazon resulted from significant reductions in autotrophic respiration indicating temporary increase in plant carbon use efficiency while NPP allocation to woody growth in drought years remained comparable to the allocation in normal years. Therefore, correcting model WBPE biases during drought years likely requires implementation of maintenance respiration down-regulation, a sink-driven growth scheme that increases priority of woody growth (Fatichi et al., 2019), and a more mechanistic module for plant nonstructural carbohydrate dynamics (Dietze et al., 2014; Martínez-Vilalta et al., 2016).

Model-data discrepancies in growth climatic sensitivity were much smaller for early-successional than for late-successional

PFTs, suggesting that early-successional trees might not be able to maintain regular stem growth in hot and dry years and therefore are more sensitive to climatic fluctuations than predicted by our model. This discrepancy could be caused by a stronger sink limitation of growth for early compared to than late-successional species during in hot and dry years. During water stress, tree growth of early-successional species could be more limited by a lack of turgor (Friend et al., 2019; Steppe et al., 2015) due to their higher hydraulic vulnerability hydraulic (Table 1). Therefore, the magnitude of the short-term increases in WBPE, which can help to maintain stem growth in hot and dry years, likely depends on plant hydraulic traits.

While annual growth records from tree rings provide the opportunity of constraining modeled growth sensitivity to interannual climatic variations, the subset of ring-forming species in tropical forests may not be fully representative of the tree community. Tropical tree species with distinct growth ring boundaries are more likely to be deciduous (Worbes, 1999), although a fair share of ring-forming species is evergreen. Among the five sampled species in our study, one is evergreen and two are brevi-deciduous (<0.5 months leafless; Vlam et al., 2014). Growth of deciduous tree species have been found to be more sensitive to moisture fluctuations (Xu et al., 2016). If the ring-forming species analyzed in our study have relatively higher sensitivity to moisture within the tree community, one would expect the community-average sensitivity to moisture should be even lower than our results based on tree ring data. Given our model is already overestimating growth sensitivity to moisture (Figure 5), this implies model biases in WBPE should be even stronger. More comprehensive high-resolution growth observations across moisture gradients are necessary to evaluate possible differences in drought responses between ring-forming and other species in tropical forests.

5 | CONCLUSIONS

The response of woody biomass production to CO_2 and climate is a major determinant of the tropical forest carbon sink under global change. Our study provides novel benchmarking options for TBM-generated woody growth using long-term tree-ring data. Our results suggest that: (1) ED2.2-hydro, a representative modern TBM, overestimates tropical woody growth sensitivity to C_a and climate, although it correctly captures C_i responses to C_a, and (2) this model-data mismatch may be resolved by incorporating WBPE responses to environmental factors (e.g., through autotrophic respiration or belowground investment). Implementing environmental constraints of WBPE based on tree-ring data would reduce the effects of CO_2 rise and hydroclimatic variability on modeled woody production. We also call for improving mechanistic representation of tree growth in TBMs by including more complete nonstructural carbohydrate dynamics and implementing sink-driven growth (Dietze et al., 2014; Fatichi et al., 2019).

More generally, our study also highlights the potential of tree-ring records to constrain TBMs' long-term woody growth predictions and reduce model uncertainty at decadal to multi-decadal timescales. In particular, tree-ring data provide novel opportunities to constrain (1) size-related changes in tree growth, (2) long-term growth responses to C_a and climate, and (3) forest biomass responses to extreme events. Yet, constraining TMBs using tree-ring data is challenging due to scale mismatches between model and data, the inherent sampling biases in data, and the influence of site-specific disturbance history (Jeong et al., 2021). Nevertheless, the increasing data availability of tropical tree-ring studies (Zuidema et al., 2022) and development of vegetation demography modules in TBMs (Fisher et al., 2018), offers exciting opportunities to produce more realistic long-term predictions of tropical forest dynamics.

ORCID
Xiangtao Xu https://orcid.org/0000-0002-9402-9474
Peter van der Sleen https://orcid.org/0000-0003-2613-2530
Peter Groenendijk https://orcid.org/0000-0003-2752-6195
Mart Vlam https://orcid.org/0000-0002-0038-6586
David Medvigy https://orcid.org/0000-0002-3076-3071

Paul Moorcroft https://orcid.org/0000-0002-2876-4673
Daniel Petticord https://orcid.org/0000-0002-1764-6321
Yixin Ma https://orcid.org/0000-0002-4454-8559
Pieter A. Zuidema https://orcid.org/0000-0001-8100-1168

REFERENCES

Ainsworth, E. A., & Long, S. P. (2005). What have we learned from 15 years of free-air CO_2 enrichment (FACE)? A meta-analytic review of the responses of photosynthesis, canopy. *New Phytologist*, *165*(2), 351–371. https://doi.org/10.1111/j.1469-8137.2004.01224.x

Anderegg, W. R. L., Schwalm, C., Biondi, F., Camarero, J. J., Koch, G., Litvak, M., Ogle, K., Shaw, J. D., Shevliakova, E., Williams, A. P., Wolf, A., Ziaco, E., & Pacala, S. (2015). Pervasive drought legacies in forest ecosystems and their implications for carbon cycle models. *Science*, *349*(6247), 528–532. https://doi.org/10.1126/science.aab1833

Anderson-Teixeira, K. J., Herrmann, V., Rollinson, C. R., Gonzalez, B., Gonzalez-Akre, E. B., Pederson, N., Alexander, M. R., Allen, C. D., Alfaro-Sánchez, R., Awada, T., Baltzer, J. L., Baker, P. J., Birch, J. D., Bunyavejchewin, S., Cherubini, P., Davies, S. J., Dow, C., Helcoski, R., Kašpar, J., … Zuidema, P. A. (2022). Joint effects of climate, tree size, and year on annual tree growth derived from tree-ring records of ten globally distributed forests. *Global Change Biology*, *28*(1), 245–266. https://doi.org/10.1111/gcb.15934

Baker, P. J., Bunyavejchewin, S., Oliver, C. D., & Ashton, P. S. (2005). Disturbance history and historical stand dynamics of a seasonal tropical forest in western Thailand. *Ecological Monographs*, *75*(3), 317–343. https://doi.org/10.1890/04-0488

Barichivich, J., Peylin, P., Launois, T., Daux, V., Risi, C., Jeong, J., & Luyssaert, S. (2021). A triple tree-ring constraint for tree growth and physiology in a global land surface model. *Biogeosciences*, *18*(12), 3781–3803. https://doi.org/10.5194/bg-18-3781-2021

Bauman, D., Fortunel, C., Cernusak, L. A., Bentley, L. P., McMahon, S. M., Rifai, S. W., Aguirre-Gutiérrez, J., Oliveras, I., Bradford, M., Laurance, S. G. W., Delhaye, G., Hutchinson, M. F., Dempsey, R., McNellis, B. E., Santos-Andrade, P. E., Ninantay-Rivera, H. R., Chambi Paucar, J. R., Phillips, O. L., & Malhi, Y. (2022). Tropical tree growth sensitivity to climate is driven by species intrinsic growth rate and leaf traits. *Global Change Biology*, *28*(4), 1414–1432. https://doi.org/10.1111/gcb.15982

Bonan, G. B., & Doney, S. C. (2018). Climate, ecosystems, and planetary futures: The challenge to predict life in earth system models. *Science*, *359*(6375), eaam8328. https://doi.org/10.1126/science.aam8328

Brienen, R. J. W., Schöngart, J., & Zuidema, P. A. (2016). Tree rings in the tropics: Insights into the ecology and climate sensitivity of tropical trees. In *Tree physiology* (Vol. 6, pp. 439–461). Springer. https://doi.org/10.1007/978-3-319-27422-5_20

Bunyavejchewin, S., LaFrankie, J. V., Baker, P. J., Davies, S. J., & Ashton, P. J. (2009). *Forest trees of Huai Kha Khaeng wildlife sanctuary, Thailand: Data from the 50-hectare forest dynamics plot*. National Parks, Wildlife & Plant Conservation Department.

Cabon, A., Kannenberg, S. A., Arain, A., Babst, F., Baldocchi, D., Belmecheri, S., Delpierre, N., Guerrieri, R., Maxwell, J. T., McKenzie, S., Meinzer, F. C., Moore, D. J. P., Pappas, C., Rocha, A. V., Szejner, P., Ueyama, M., Ulrich, D., Vincke, C., Voelker, S. L., … Anderegg, W. R. L. (2022). Cross-biome synthesis of source versus sink limits to tree growth. *Science*, *376*(6594), 758–761. https://doi.org/10.1126/science.abm4875

Camac, J. S., Condit, R., FitzJohn, R. G., McCalman, L., Steinberg, D., Westoby, M., Wright, S. J., & Falster, D. S. (2018). Partitioning mortality into growth-dependent and growth-independent hazards across 203 tropical tree species. *Proceedings of the National Academy of Sciences of the United States of America*, *115*(49), 12459–12464. https://doi.org/10.1073/pnas.1721040115

Cernusak, L. A., Winter, K., Dalling, J. W., Holtum, J. A. M., Jaramillo, C., Korner, C., Leakey, A. D. B., Norby, R. J., Poulter, B., Turner, B. L., & Wright, S. J. (2013). Tropical forest responses to increasing atmospheric CO_2: Current knowledge and opportunities for future research. *Functional Plant Biology*, *40*(6), 531–551. https://doi.org/10.1071/fp12309

Chave, J., Andalo, C., Brown, S., Cairns, M. A., Chambers, J. Q., Eamus, D., Fölster, H., Fromard, F., Higuchi, N., Kira, T., Lescure, J. P., Nelson, B. W., Ogawa, H., Puig, H., Riéra, B., & Yamakura, T. (2005). Tree allometry and improved estimation of carbon stocks and balance in tropical forests. *Oecologia*, *145*(1), 87–99. https://doi.org/10.1007/s00442-005-0100-x

Chave, J., Condit, R., Muller-Landau, H. C., Thomas, S. C., Ashton, P. S., Bunyavejchewin, S., Co, L. L., Dattaraja, H. S., Davies, S. J., Esufali, S., Ewango, C. E. N., Feeley, K. J., Foster, R. B., Gunatilleke, N., Gunatilleke, S., Hall, P., Hart, T. B., Hernández, C., Hubbell, S. P., … Losos, E. C. (2008). Assessing evidence for a pervasive alteration in tropical tree communities. *PLoS Biology*, *6*(3), 455–462. https://doi.org/10.1371/journal.pbio.0060045

Collalti, A., Ibrom, A., Stockmarr, A., Cescatti, A., Alkama, R., Fernández-Martínez, M., Matteucci, G., Sitch, S., Friedlingstein, P., Ciais, P., Goll, D. S., Nabel, J. E. M. S., Pongratz, J., Arneth, A., Haverd, V., & Prentice, I. C. (2020). Forest production efficiency increases with growth temperature. *Nature Communications*, *11*(1), 1–9. https://doi.org/10.1038/s41467-020-19187-w

Collalti, A., & Prentice, I. C. (2019). Is NPP proportional to GPP? Waring's hypothesis 20 years on. *Tree Physiology*, *39*(8), 1473–1483. https://doi.org/10.1093/treephys/tpz034

Cunha, H. F. V., Andersen, K. M., Lugli, L. F., Santana, F. D., Aleixo, I. F., Moraes, A. M., Garcia, S., Di Ponzio, R., Mendoza, E. O., Brum, B., Rosa, J. S., Cordeiro, A. L., Portela, B. T. T., Ribeiro, G., Coelho, S. D., de Souza, S. T., Silva, L. S., Antonieta, F., Pires, M., … Quesada, C. A. (2022). Direct evidence for phosphorus limitation on Amazon forest productivity. *Nature*, *608*(7923), 558–562. https://doi.org/10.1038/s41586-022-05085-2

Dietze, M. C., Sala, A., Carbone, M. S., Czimczik, C. I., Mantooth, J. A., Richardson, A. D., & Vargas, R. (2014). Nonstructural carbon in woody plants. *Annual Review of Plant Biology*, *65*(1), 667–687. https://doi.org/10.1146/annurev-arplant-050213-040054

Doughty, C. E., Metcalfe, D. B., Girardin, C. A. J., Amézquita, F. F., Cabrera, D. G., Huasco, W. H., Silva-Espejo, J. E., Araujo-Murakami, A., Da Costa, M. C., Rocha, W., Feldpausch, T. R., Mendoza, A. L. M., Da Costa, A. C. L., Meir, P., Phillips, O. L., & Malhi, Y. (2015). Drought impact on forest carbon dynamics and fluxes in Amazonia. *Nature*, *519*(7541), 78–82. https://doi.org/10.1038/nature14213

Eckes-Shephard, A. H., Tiavlovsky, E., Chen, Y., Fonti, P., & Friend, A. D. (2021). Direct response of tree growth to soil water and its implications for terrestrial carbon cycle modelling. *Global Change Biology*, *27*(1), 121–135. https://doi.org/10.1111/gcb.15397

Fatichi, S., Pappas, C., Zscheischler, J., & Leuzinger, S. (2019). Modelling carbon sources and sinks in terrestrial vegetation. *New Phytologist*, *221*(2), 652–668. https://doi.org/10.1111/nph.15451

Fauset, S., Oliveira, L., Buckeridge, M. S., Foyer, C. H., Galbraith, D., Tiwari, R., & Gloor, M. (2019). Contrasting responses of stomatal conductance and photosynthetic capacity to warming and elevated CO_2 in the tropical tree species *Alchornea glandulosa* under heatwave conditions. *Environmental and Experimental Botany*, *158*, 28–39. https://doi.org/10.1016/j.envexpbot.2018.10.030

Fisher, R. A., & Koven, C. D. (2020). Perspectives on the future of land surface models and the challenges of representing complex terrestrial systems. *Journal of Advances in Modeling Earth Systems*, *12*(4), e2018MS001453. https://doi.org/10.1029/2018ms001453

Fisher, R. A., Koven, C. D., Anderegg, W. R. L., Christoffersen, B. O., Dietze, M. C., Farrior, C. E., Holm, J. A., Hurtt, G. C., Knox, R. G., Lawrence, P. J., Lichstein, J. W., Longo, M., Matheny, A. M., Medvigy, D., Muller-Landau, H. C., Powell, T. L., Serbin, S. P., Sato, H., Shuman, J. K., … Moorcroft, P. R. (2018). Vegetation demographics in earth system models: A review of progress and priorities. *Global Change Biology*, 24(1), 35–54. https://doi.org/10.1111/gcb.13910

Fleischer, K., Rammig, A., De Kauwe, M. G., Walker, A. P., Domingues, T. F., Fuchslueger, L., Garcia, S., Goll, D. S., Grandis, A., Jiang, M., Haverd, V., Hofhansl, F., Holm, J. A., Kruijt, B., Leung, F., Medlyn, B. E., Mercado, L. M., Norby, R. J., Pak, B., … Lapola, D. M. (2019). Amazon forest response to CO_2 fertilization dependent on plant phosphorus acquisition. *Nature Geoscience*, 12(9), 736–741. https://doi.org/10.1038/s41561-019-0404-9

Fleischer, K., & Terrer, C. (2022). Estimates of soil nutrient limitation on the CO_2 fertilization effect for tropical vegetation. *Global Change Biology*, 28, 6366–6369. https://doi.org/10.1111/GCB.16377

Friend, A. D., Eckes-Shephard, A. H., Fonti, P., Rademacher, T. T., Rathgeber, C. B. K., Richardson, A. D., & Turton, R. H. (2019). On the need to consider wood formation processes in global vegetation models and a suggested approach. *Annals of Forest Science*, 76(2), 1–13. https://doi.org/10.1007/s13595-019-0819-x

Friend, A. D., Stevens, A. K., Knox, R. G., & Cannell, M. G. R. (1997). A process-based, terrestrial biosphere model of ecosystem dynamics (hybrid v3.0). *Ecological Modelling*, 95(2–3), 249–287. https://doi.org/10.1016/S0304-3800(96)00034-8

Groenendijk, P., van der Sleen, P., Vlam, M., Bunyavejchewin, S., Bongers, F., & Zuidema, P. A. (2015). No evidence for consistent long-term growth stimulation of 13 tropical tree species: Results from tree-ring analysis. *Global Change Biology*, 21(10), 3762–3776. https://doi.org/10.1111/gcb.12955

Grossman, D. (2016). Amazon rainforest to get a growth check. *Science*, 352(6286), 635–636. https://doi.org/10.1126/science.352.6286.635

Haverd, V., Smith, B., Canadell, J. G., Cuntz, M., Mikaloff-Fletcher, S., Farquhar, G., Woodgate, W., Briggs, P. R., & Trudinger, C. M. (2020). Higher than expected CO_2 fertilization inferred from leaf to global observations. *Global Change Biology*, 26(4), 2390–2402. https://doi.org/10.1111/gcb.14950

Hickler, T., Rammig, A., & Werner, C. (2015). Modelling CO_2 impacts on forest productivity. *Current Forestry Reports*, 1(2), 69–80. https://doi.org/10.1007/s40725-015-0014-8

Holbrook, N. M., & Putz, F. E. (1989). Influence of neighbors on tree form: Effects of lateral shade and prevention of sway on the allometry of Liquidambar styraciflua (sweet gum). *American Journal of Botany*, 76(12), 1740–1749. https://doi.org/10.2307/2444473

Hubau, W., Lewis, S. L., Phillips, O. L., Affum-Baffoe, K., Beeckman, H., Cuní-Sanchez, A., Daniels, A. K., Ewango, C. E. N., Fauset, S., Mukinzi, J. M., Sheil, D., Sonké, B., Sullivan, M. J. P., Sunderland, T. C. H., Taedoumg, H., Thomas, S. C., White, L. J. T., Abernethy, K. A., Adu-Bredu, S., … Zemagho, L. (2020). Asynchronous carbon sink saturation in African and Amazonian tropical forests. *Nature*, 579(7797), 80–87. https://doi.org/10.1038/s41586-020-2035-0

Huete, A. R., Restrepo-Coupe, N., Ratana, P., Didan, K., Saleska, S. R., Ichii, K., Panuthai, S., & Gamo, M. (2008). Multiple site tower flux and remote sensing comparisons of tropical forest dynamics in monsoon Asia. *Agricultural and Forest Meteorology*, 148(5), 748–760. https://doi.org/10.1016/j.agrformet.2008.01.012

Huntingford, C., Zelazowski, P., Galbraith, D., Mercado, L. M., Sitch, S., Fisher, R., Lomas, M., Walker, A. P., Jones, C. D., Booth, B. B. B., Malhi, Y., Hemming, D., Kay, G., Good, P., Lewis, S. L., Phillips, O. L., Atkin, O. K., Lloyd, J., Gloor, E., … Cox, P. M. (2013). Simulated resilience of tropical rainforests to CO_2-induced climate change. *Nature Geoscience*, 6(4), 268–273. https://doi.org/10.1038/ngeo1741

Jeong, J., Barichivich, J., Peylin, P., Haverd, V., McGrath, M. J., Vuichard, N., Evans, M. N., Babst, F., & Luyssaert, S. (2021). Using the International Tree-Ring Data Bank (ITRDB) records as century-long benchmarks for global land-surface models. *Geoscientific Model Development*, 14(9), 5891–5913. https://doi.org/10.5194/gmd-14-5891-2021

Jiang, M., Medlyn, B. E., Drake, J. E., Duursma, R. A., Anderson, I. C., Barton, C. V. M., Boer, M. M., Carrillo, Y., Castañeda-Gómez, L., Collins, L., Crous, K. Y., De Kauwe, M. G., dos Santos, B. M., Emmerson, K. M., Facey, S. L., Gherlenda, A. N., Gimeno, T. E., Hasegawa, S., Johnson, S. N., … Ellsworth, D. S. (2020). The fate of carbon in a mature forest under carbon dioxide enrichment. *Nature*, 580(7802), 227–231. https://doi.org/10.1038/s41586-020-2128-9

Katul, G., Manzoni, S., Palmroth, S., & Oren, R. (2010). A stomatal optimization theory to describe the effects of atmospheric CO_2 on leaf photosynthesis and transpiration. *Annals of Botany*, 105(3), 431–442. https://doi.org/10.1093/aob/mcp292

Kim, D., Medvigy, D., Maier, C. A., Johnsen, K., & Palmroth, S. (2020). Biomass increases attributed to both faster tree growth and altered allometric relationships under long-term carbon dioxide enrichment at a temperate forest. *Global Change Biology*, 26(4), 2519–2533. https://doi.org/10.1111/gcb.14971

Klesse, S., Babst, F., Lienert, S., Spahni, R., Joos, F., Bouriaud, O., Carrer, M., Di Filippo, A., Poulter, B., Trotsiuk, V., Wilson, R., & Frank, D. C. (2018). A combined tree ring and vegetation model assessment of European forest growth sensitivity to interannual climate variability. *Global Biogeochemical Cycles*, 32(8), 1226–1240. https://doi.org/10.1029/2017GB005856

Levy-Varon, J. H., Batterman, S. A., Medvigy, D., Xu, X., Hall, J. S., van Breugel, M., & Hedin, L. O. (2019). Tropical carbon sink accelerated by symbiotic dinitrogen fixation. *Nature Communications*, 10(1), 5637. https://doi.org/10.1038/s41467-019-13656-7

Longo, M., Knox, R. G., Medvigy, D. M., Levine, N. M., Dietze, M. C., Kim, Y., Swann, A. L. S., Zhang, K., Rollinson, C. R., Bras, R. L., Wofsy, S. C., & Moorcroft, P. R. (2019). The biophysics, ecology, and biogeochemistry of functionally diverse, vertically and horizontally heterogeneous ecosystems: The ecosystem demography model, version 2.2-part 1: Model description. *Geoscientific Model Development*, 12(10), 4309–4346. https://doi.org/10.5194/gmd-12-4309-2019

Longo, M., Saatchi, S., Keller, M., Bowman, K., Ferraz, A., Moorcroft, P. R., Morton, D. C., Bonal, D., Brando, P., Burban, B., Derroire, G., Dos-Santos, M. N., Meyer, V., Saleska, S., Trumbore, S., & Vincent, G. (2020). Impacts of degradation on water, energy, and carbon cycling of the Amazon tropical forests. *Journal of Geophysical Research: Biogeosciences*, 125(8), e2020JG005677. https://doi.org/10.1029/2020jg005677

Manzoni, S., Vico, G., Palmroth, S., Porporato, A., & Katul, G. (2013). Optimization of stomatal conductance for maximum carbon gain under dynamic soil moisture. *Advances in Water Resources*, 62, 90–105. https://doi.org/10.1016/j.advwatres.2013.09.020

Martínez-Vilalta, J., Sala, A., Asensio, D., Galiano, L., Hoch, G., Palacio, S., Piper, F. I., & Lloret, F. (2016). Dynamics of non-structural carbohydrates in terrestrial plants: A global synthesis. *Ecological Monographs*, 86(4), 495–516. https://doi.org/10.1002/ecm.1231

McCarroll, D., & Loader, N. J. (2004). Stable isotopes in tree rings. *Quaternary Science Reviews*, 23(7–8), 771–801. https://doi.org/10.1016/j.quascirev.2003.06.017

McDowell, N. G., Allen, C. D., Anderson-Teixeira, K., Aukema, B. H., Bond-Lamberty, B., Chini, L., Clark, J. S., Dietze, M., Grossiord, C., Hanbury-Brown, A., Hurtt, G. C., Jackson, R. B., Johnson, D. J., Kueppers, L., Lichstein, J. W., Ogle, K., Poulter, B., Pugh, T. A. M., Seidl, R., … Xu, C. (2020). Pervasive shifts in forest dynamics in a changing world. *Science*, 368(6494), eaaz9463. https://doi.org/10.1126/science.aaz9463

Medvigy, D., Wang, G., Zhu, Q., Riley, W. J., Trierweiler, A. M., Waring, B. G., Xu, X., & Powers, J. S. (2019). Observed variation in soil

properties can drive large variation in modelled forest functioning and composition during tropical forest secondary succession. *New Phytologist*, 223(4), 1820–1833. https://doi.org/10.1111/nph.15848

Medvigy, D., Wofsy, S. C., Munger, J. W., Hollinger, D. Y., & Moorcroft, P. R. (2009). Mechanistic scaling of ecosystem function and dynamics in space and time: Ecosystem Demography model version 2. *Journal of Geophysical Research: Biogeosciences*, 114(1), G01002. https://doi.org/10.1029/2008JG000812

Mendivelso, H. A., Camarero, J. J., Obregon, O. R., Gutierrez, E., & Toledo, M. (2013). Differential growth responses to water balance of coexisting deciduous tree species are linked to wood density in a Bolivian tropical dry forest. *PLoS ONE*, 8(10), e73855. https://doi.org/10.1371/journal.pone.0073855

Metcalfe, D. B., Meir, P., Aragão, L. E. O. C., Lobo-do-Vale, R., Galbraith, D., Fisher, R. A., Chaves, M. M., Maroco, J. P., da Costa, A. C. L., de Almeida, S. S., Braga, A. P., Gonçalves, P. H. L., de Athaydes, J., da Costa, M., Portela, T. T. B., de Oliveira, A. A. R., Malhi, Y., & Williams, M. (2010). Shifts in plant respiration and carbon use efficiency at a large-scale drought experiment in the eastern Amazon. *New Phytologist*, 187(3), 608–621. https://doi.org/10.1111/j.1469-8137.2010.03319.x

Moorcroft, P. R., Hurtt, G. C., & Pacala, S. W. (2001). A method for scaling vegetation dynamics: The ecosystem demography model (ED). *Ecological Monographs*, 71(4), 557–585. https://doi.org/10.1890/0012-9615(2001)071[0557:Amfsvd]2.0.Co;2

Nock, C. A., Geihofer, D., Grabner, M., Baker, P. J., Bunyavejchewin, S., & Hietz, P. (2009). Wood density and its radial variation in six canopy tree species differing in shade-tolerance in western Thailand. *Annals of Botany*, 104(2), 297–306. https://doi.org/10.1093/aob/mcp118

Norby, R. J., & Zak, D. R. (2011). Ecological lessons from Free-Air CO_2 Enrichment (FACE) experiments. *Annual Review of Ecology, Evolution, and Systematics*, 42(42), 181–203.

Palacio, S., Hoch, G., Sala, A., Körner, C., & Millard, P. (2014). Does carbon storage limit tree growth? *New Phytologist*, 201(4), 1096–1100. https://doi.org/10.1111/NPH.12602

Pan, Y., Birdsey, R. A., Fang, J., Houghton, R., Kauppi, P. E., Kurz, W. A., Phillips, O. L., Shvidenko, A., Lewis, S. L., Canadell, J. G., Ciais, P., Jackson, R. B., Pacala, S. W., McGuire, A. D., Piao, S., Rautiainen, A., Sitch, S., & Hayes, D. (2011). A large and persistent carbon sink in the world's forests. *Science*, 333(6045), 988–993. https://doi.org/10.1126/science.1201609

Peltier, D. M. P., & Ogle, K. (2020). Tree growth sensitivity to climate is temporally variable. *Ecology Letters*, 23(11), 1561–1572. https://doi.org/10.1111/ele.13575

Peters, R. L., Groenendijk, P., Vlam, M., & Zuidema, P. A. (2015). Detecting long-term growth trends using tree rings: A critical evaluation of methods. *Global Change Biology*, 21(5), 2040–2054. https://doi.org/10.1111/gcb.12826

Piao, S., Wang, X., Wang, K., Li, X., Bastos, A., Canadell, J. G., Ciais, P., Friedlingstein, P., & Sitch, S. (2020). Interannual variation of terrestrial carbon cycle: Issues and perspectives. *Global Change Biology*, 26(1), 300–318. https://doi.org/10.1111/gcb.14884

Pugh, T. A. M., Lindeskog, M., Smith, B., Poulter, B., Arneth, A., Haverd, V., & Calle, L. (2019). Role of forest regrowth in global carbon sink dynamics. *Proceedings of the National Academy of Sciences of the United States of America*, 116(10), 4382–4387. https://doi.org/10.1073/pnas.1810512116

Rammig, A., Wiedermann, M., Donges, J. F., Babst, F., Von Bloh, W., Frank, D., Thonicke, K., & Mahecha, M. D. (2015). Coincidences of climate extremes and anomalous vegetation responses: Comparing tree ring patterns to simulated productivity. *Biogeosciences*, 12(2), 373–385. https://doi.org/10.5194/bg-12-373-2015

Sala, A., Woodruff, D. R., & Meinzer, F. C. (2012). Carbon dynamics in trees: Feast or famine? *Tree Physiology*, 32(6), 764–775. https://doi.org/10.1093/treephys/tpr143

Seabold, S., & Perktold, J. (2010). Statsmodels: Econometric and statistical modeling with python. *Proceedings of the 9th python in science conference.* https://doi.org/10.25080/majora-92bf1922-011

Sheffield, J., Goteti, G., & Wood, E. F. (2006). Development of a 50-year high-resolution global dataset of meteorological forcings for land surface modeling. *Journal of Climate*, 19(13), 3088–3111. https://doi.org/10.1175/Jcli3790.1

Sitch, S., Huntingford, C., Gedney, N., Levy, P. E., Lomas, M., Piao, S. L., Betts, R., Ciais, P., Cox, P., Friedlingstein, P., Jones, C. D., Prentice, I. C., & Woodward, F. I. (2008). Evaluation of the terrestrial carbon cycle, future plant geography and climate-carbon cycle feedbacks using five Dynamic Global Vegetation Models (DGVMs). *Global Change Biology*, 14(9), 2015–2039. https://doi.org/10.1111/j.1365-2486.2008.01626.x

Slot, M., Rifai, S. W., & Winter, K. (2021). Photosynthetic plasticity of a tropical tree species, *Tabebuia rosea*, in response to elevated temperature and [CO_2]. *Plant, Cell & Environment*, 44(7), 2347–2364. https://doi.org/10.1111/pce.14049

Smith-Martin, C. M., Xu, X., Medvigy, D., Schnitzer, S. A., & Powers, J. S. (2020). Allometric scaling laws linking biomass and rooting depth vary across ontogeny and functional groups in tropical dry forest lianas and trees. *New Phytologist*, 226(3), 714–726. https://doi.org/10.1111/nph.16275

Steppe, K., Sterck, F., & Deslauriers, A. (2015). Diel growth dynamics in tree stems: Linking anatomy and ecophysiology. *Trends in Plant Science*, 20(6), 335–343. https://doi.org/10.1016/j.tplants.2015.03.015

Terrer, C., Jackson, R. B., Prentice, I. C., Keenan, T. F., Kaiser, C., Vicca, S., Fisher, J. B., Reich, P. B., Stocker, B. D., Hungate, B. A., Peñuelas, J., McCallum, I., Soudzilovskaia, N. A., Cernusak, L. A., Talhelm, A. F., Van Sundert, K., Piao, S., Newton, P. C. D., Hovenden, M. J., … Franklin, O. (2019). Nitrogen and phosphorus constrain the CO_2 fertilization of global plant biomass. *Nature Climate Change*, 9(9), 684–689. https://doi.org/10.1038/s41558-019-0545-2

Van Der Sleen, P., Groenendijk, P., Vlam, M., Anten, N. P. R., Boom, A., Bongers, F., Pons, T. L., Terburg, G., & Zuidema, P. A. (2015). No growth stimulation of tropical trees by 150 years of CO_2 fertilization but water-use efficiency increased. *Nature Geoscience*, 8(1), 24–28. https://doi.org/10.1038/ngeo2313

van der Sleen, P., Zuidema, P. A., & Pons, T. L. (2017). Stable isotopes in tropical tree rings: Theory, methods and applications. *Functional Ecology*, 31(9), 1674–1689. https://doi.org/10.1111/1365-2435.12889

Vicca, S., Luyssaert, S., Peñuelas, J., Campioli, M., Chapin, F. S., Ciais, P., Heinemeyer, A., Högberg, P., Kutsch, W. L., Law, B. E., Malhi, Y., Papale, D., Piao, S. L., Reichstein, M., Schulze, E. D., & Janssens, I. A. (2012). Fertile forests produce biomass more efficiently. *Ecology Letters*, 15(6), 520–526. https://doi.org/10.1111/j.1461-0248.2012.01775.x

Vlam, M., Baker, P. J., Bunyavejchewin, S., & Zuidema, P. A. (2014). Temperature and rainfall strongly drive temporal growth variation in Asian tropical forest trees. *Oecologia*, 174(4), 1449–1461. https://doi.org/10.1007/s00442-013-2846-x

Vlam, M., van der Sleen, P., Groenendijk, P., & Zuidema, P. A. (2017). Tree age distributions reveal large-scale disturbance-recovery cycles in three tropical forests. *Frontiers in Plant Science*, 7, 1984. https://doi.org/10.3389/fpls.2016.01984

Walker, A. P., De Kauwe, M. G., Bastos, A., Belmecheri, S., Georgiou, K., Keeling, R. F., McMahon, S. M., Medlyn, B. E., Moore, D. J. P., Norby, R. J., Zaehle, S., Anderson-Teixeira, K. J., Battipaglia, G., Brienen, R. J. W., Cabugao, K. G., Cailleret, M., Campbell, E., Canadell, J.

G., Ciais, P., … Zuidema, P. A. (2021). Integrating the evidence for a terrestrial carbon sink caused by increasing atmospheric CO_2. *New Phytologist*, 229(5), 2413–2445. https://doi.org/10.1111/nph.16866

Waring, B. G., Pérez-Aviles, D., Murray, J. G., & Powers, J. S. (2019). Plant community responses to stand-level nutrient fertilization in a secondary tropical dry forest. *Ecology*, 100(6), e02691. https://doi.org/10.1002/ecy.2691

Williams, L. J., Bunyavejchewin, S., & Baker, P. J. (2008). Deciduousness in a seasonal tropical forest in western Thailand: Interannual and intraspecific variation in timing, duration and environmental cues. *Oecologia*, 155(3), 571–582. https://doi.org/10.1007/s00442-007-0938-1

Worbes, M. (1999). Annual growth rings, rainfall-dependent growth and long-term growth patterns of tropical trees from the Caparo Forest Reserve in Venezuela. *Journal of Ecology*, 87(3), 391–403. https://doi.org/10.1046/j.1365-2745.1999.00361.x

Wright, S. J. (2019). Plant responses to nutrient addition experiments conducted in tropical forests. *Ecological Monographs*, 89(4), e01382. https://doi.org/10.1002/ecm.1382

Xu, X., Konings, A. G., Longo, M., Feldman, A., Xu, L., Saatchi, S., Wu, D., Wu, J., & Moorcroft, P. (2021). Leaf surface water, not plant water stress, drives diurnal variation in tropical forest canopy water content. *New Phytologist*, 231(1), 122–136. https://doi.org/10.1111/nph.17254

Xu, X., Medvigy, D., Powers, J. S., Becknell, J. M., & Guan, K. (2016). Diversity in plant hydraulic traits explains seasonal and inter-annual variations of vegetation dynamics in seasonally dry tropical forests. *The New Phytologist*, 212(1), 80–95. https://doi.org/10.1111/nph.14009

Xu, X., & Trugman, A. T. (2021). Trait-based modeling of terrestrial ecosystems: Advances and challenges under global change. *Current Climate Change Reports*, 7(1), 1–13. https://doi.org/10.1007/s40641-020-00168-6

Zuidema, P. A., Babst, F., Groenendijk, P., Trouet, V., Abiyu, A., Acuña-Soto, R., Adenesky-Filho, E., Alfaro-Sánchez, R., Aragão, J. R. V., Assis-Pereira, G., Bai, X., Barbosa, A. C., Battipaglia, G., Beeckman, H., Botosso, P. C., Bradley, T., Bräuning, A., Brienen, R., Buckley, B. M., … Zhou, Z. K. (2022). Tropical tree growth driven by dry-season climate variability. *Nature Geoscience*, 15(4), 269–276. https://doi.org/10.1038/s41561-022-00911-8

Zuidema, P. A., Poulter, B., & Frank, D. C. (2018). A wood biology agenda to support global vegetation modelling. *Trends in Plant Science*, 23(11), 1006–1015. https://doi.org/10.1016/j.tplants.2018.08.003

Zuleta, D., Arellano, G., McMahon, S. M., Aguilar, S., Bunyavejchewin, S., Castaño, N., Chang-Yang, C. H., Duque, A., Mitre, D., Nasardin, M., Pérez, R., Sun, I. F., Yao, T. L., Valencia, R., Krishna Moorthy, S. M., Verbeeck, H., & Davies, S. J. (2023). Damage to living trees contributes to almost half of the biomass losses in tropical forests. *Global Change Biology*, 29, 3409–3420. https://doi.org/10.1111/GCB.16687

Zweifel, R., Sterck, F., Braun, S., Buchmann, N., Eugster, W., Gessler, A., Häni, M., Peters, R. L., Walthert, L., Wilhelm, M., Ziemińska, K., & Etzold, S. (2021). Why trees grow at night. *New Phytologist*, 231, 2174–2185. https://doi.org/10.1111/NPH.17552

SUPPORTING INFORMATION

Additional supporting information can be found online in the Supporting Information section at the end of this article.